



# Exhumation and preservation of the Tianyu Cu-Ni deposit constrained by low-temperature thermochronology: Insights into the thermo-tectonic history of the Chinese Eastern Tianshan

Meng Luo <sup>a,d</sup>, Zhiyuan He <sup>b</sup>, Fujun Wang <sup>a</sup>, Wenbin Zhu <sup>a,c,\*</sup>, Guangwei Li <sup>a,c</sup>, Johan De Grave <sup>b</sup>, Yiqiong Wang <sup>a</sup>, Bihai Zheng <sup>a</sup>, Yueqiao Zhang <sup>a</sup>

<sup>a</sup> State Key Laboratory for Mineral Deposits Research, School of Earth Sciences and Engineering, Nanjing University, 210023 Nanjing, China

<sup>b</sup> Laboratory for Mineralogy and Petrology, Department of Geology, Ghent University, Krijgslaan 281 S8, 9000 Ghent, Belgium

<sup>c</sup> Institute of Continental Geodynamics, Nanjing University, 210023 Nanjing, China

<sup>d</sup> School of Civil Engineering, Wanjiang University of Technology, 243031 Ma'anshan, China



## ARTICLE INFO

### Keywords:

Low-temperature thermochronology  
Tianyu Cu-Ni deposit  
Exhumation and preservation  
Eastern Tianshan

## ABSTRACT

The Chinese Eastern Tianshan is an important metallogenic region where major Cu-Ni ores are mined. Previous research in the region primarily focused on the ore genesis. Precise thermochronological data to constrain the exhumation history and preservation of the ore deposits are limited at best. Tianyu is one of these Cu-Ni deposits in the area. Here we present new low-temperature thermochronological data to contribute to the understanding of its exhumation and preservation history. Zircon (U-Th)/He ages of ~ 134–69 Ma, apatite fission track ages of ~ 100–75 Ma, and apatite (U-Th)/He ages of ~ 117–38 Ma from five granodiorite samples of the ore wall rock at different depths of a borehole in the Tianyu deposit were obtained. Our thermochronological data and inverse thermal history modeling reveal a moderate to rapid and final basement cooling phase during the Cretaceous (~115–85 Ma) with an averaged cooling rate of ~ 3–4 °C/Ma. It is envisaged that this phase eventually exposed the ore deposits and that posterior erosion was limited, contributing to the preservation of the deposit. Combined with previously published geochronological and thermochronological data, a multi-stage cooling history of the ore bearing host rocks can be established. After its late Permian (~280–260 Ma) magmatic-hydrothermal formation, two phases of accelerated regional cooling (i.e., in the late Permian-Early Triassic, ~260–240 Ma; and the mid-Cretaceous, ~115–85 Ma) can be recognized. The more intense Cretaceous cooling is associated with the ore body finally being exhumed to the surface, and provides essential information for ore exploration in the region. Further, we propose that areas in the Eastern Tianshan with similar thermal histories to the Tianyu Cu-Ni deposit may be potential exploration targets.

## 1. Introduction

Low-temperature thermochronological methods, such as zircon and apatite (U-Th)/He (ZHe and AHe) and apatite fission track (AFT) dating, measure the timing and rates at which rocks approach the upper crust and surface, and cool as a result of exhumation. These methods hence provide constraints on the thermal history of a geological unit when it passes through the shallow crustal isothermal structure from ~ 200 to ~ 45 °C, and are used to reveal the complex dynamic mechanisms during this process (e.g., Gallagher et al., 1998; Reiners and Brandon, 2006;

Enkelmann and Garver, 2016). One important application of low-temperature thermochronology is to reconstruct the post-mineralization thermal history of ore deposits (Márton et al., 2010), which would be helpful to evaluate their preservation potential. In addition, combined with medium- to high-temperature geo/thermochronometry such as biotite and muscovite  $^{40}\text{Ar}/^{39}\text{Ar}$  and zircon U-Pb dating, a comprehensive cooling history since the formation of the ores can be derived (e.g., Evans et al., 2013; Zhang et al., 2017). The formation of an economic mineral deposit requires not only a genetic process but also later exhumation events that make it possible for

\* Corresponding author at: State Key Laboratory for Mineral Deposits Research, School of Earth Sciences and Engineering, Nanjing University, 210023 Nanjing, China.

E-mail address: [zwb@nju.edu.cn](mailto:zwb@nju.edu.cn) (W. Zhu).

commercial mining (Zhai et al., 2000; Wang et al., 2008), and thus understanding the post-mineralization thermo-tectonic evolution of the ore deposits and/or their host rocks, is crucial for regional exploration targeting.

The Central Asian Orogenic Belt (CAOB) is one of the largest accretionary orogens on Earth (Fig. 1A). Its development initiated in the Neoproterozoic, and this vast orogenic system further grew during the Paleozoic via the accretion of various island arcs, seamounts, accretionary wedges and micro-continents (e.g., Xiao et al., 2003; Jahn et al., 2004; Windley et al., 2007; Wilhem et al., 2012), accompanied by voluminous magmatism and large-scale mineralization (Wan et al., 2017; Gao et al., 2018). These magmatic activities have been closely related with the formation of massive ore deposits whose multi-stage metallogenic ages vary from the Early Ordovician to Late Cretaceous (e.g., Heinhorst et al., 2000; Yakubchuk, 2004; Seltmann et al., 2014; Zeng et al., 2015; Shen et al., 2016). Located in the southwestern CAOB, the Tianshan belt extends ~ E-W across the Central Asian republics and NW China (Fig. 1B). It is one of the largest gold provinces in the world (e.g., Mao et al., 2004), and is a critical Cu-Ni metallogenic belt (e.g., Mao et al., 2008; Pirajno, 2010). The eastern segment of the Tianshan belt in China (herein referred to as the Eastern Tianshan; Fig. 1B) hosts numerous gold deposits (Mao et al., 2004; Chen et al., 2012; Muhtar et al., 2020), and several magmatic Cu-Ni sulfide deposits (Zhou et al., 2004; Qin et al., 2011; Wu et al., 2018). Many of these Au and Cu-Ni sulfide deposits are spatio-temporally associated with each other, and structurally controlled by several near parallel east-trending faults (Pirajno, 2010; Wang et al., 2014). Previous studies largely focus on the tectonic setting, geodynamic processes and metallogenesis of these Paleozoic Eastern Tianshan ore deposits (refer to Gao et al. (2018) and Xiao et al. (2020) for recent reviews), however, little attention has been paid to their long-term post-mineralization evolution (i.e., their exhumation and preservation).

It is clear that understanding the exhumation history of the host rocks of the deposits has valuable implications for deeper insights into the preservation and exposure of the mineral systems in the Eastern Tianshan. In this contribution, we focus on the thermal history of the

Tianyu Cu-Ni sulfide deposit that is situated in the central part of the Eastern Tianshan metallogenic belt (Fig. 2). Granitoid wall rock samples from a borehole section are analyzed by low-temperature thermochronological techniques, including zircon (U-Th)/He (ZHe), apatite fission track (AFT) and apatite (U-Th)/He (AHe) dating, and their integrated thermal history is derived by associated inverse modeling. In addition, according to compiled thermochronological data from the region, we further explore the intra-continental tectonics of the Eastern Tianshan and its neighboring regions, in order to shed further light on the Paleozoic ore deposits exploration in the Eastern Tianshan.

## 2. Geological background

### 2.1. Regional geology of the Eastern Tianshan

The Chinese part of the Tianshan belt is geographically divided into western and eastern segments along longitude ~ 89° E. The Chinese Eastern Tianshan is further divided into three tectonic units as the North, Central and South Tianshan based on differences in basement nature (Shu et al., 2004; Xiao et al., 2004; Charvet et al., 2007). They are separated from each other by two deep-rooted strike-slip faults (i.e., the Main Tianshan shear zone and the Kumishi - Kawabulak - Xingxingxia fault; Fig. 1B) (He et al., 2021a).

The Chinese North Tianshan represents a remnant Paleozoic accretionary complex (Wang et al., 2006; Han et al., 2010a). This tectonic unit contains a series of island arcs (e.g., the Bogda-Harlik, Dananhua and Yamansu arcs) that mainly consist of late Paleozoic sedimentary-volcanic strata and granitic rocks (Xiao et al., 2009; Zhang et al., 2016), and host a variety of porphyry Cu, Cu-Ni, orogenic Au and skarn-type Fe deposits (e.g., Qin et al., 2011; Mao et al., 2015; Xiao et al., 2017). In the Permian, the southern part of the North Tianshan was subjected to large-scale post-collisional dextral transcurrent tectonics (Wang et al., 2008, 2014). The South Tianshan is a continuous orogenic belt along-strike, and marks a Carboniferous suture formed by the collision of the Tarim craton with the aforementioned northern blocks (Wang et al., 2011; Han and Zhao, 2018; Zhong et al., 2019). This belt

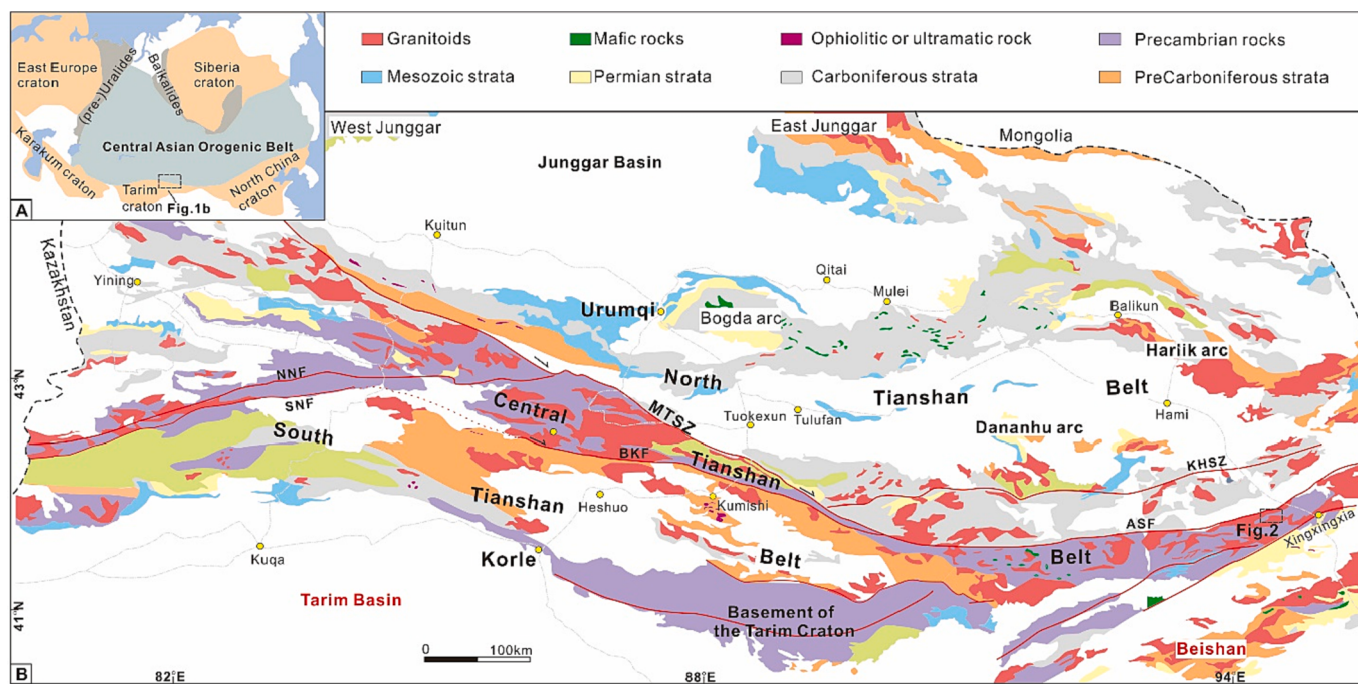


**Fig. 1.** (A) Tectonic sketch map of Central Asia showing the main tectonic units and the location of the Eastern Tianshan (modified after Xiao et al., 2004). (B) Simplified geological map of the Chinese Tianshan Orogen (modified after Li et al., 2020). MTSZ: Main Tianshan Shear Zone; KHSZ: Kanggur-Huangshan Shear Zone; BKF: Baluntai-Kumishi Fault; ASF: Aqikekudu-Shaquanzi Fault.

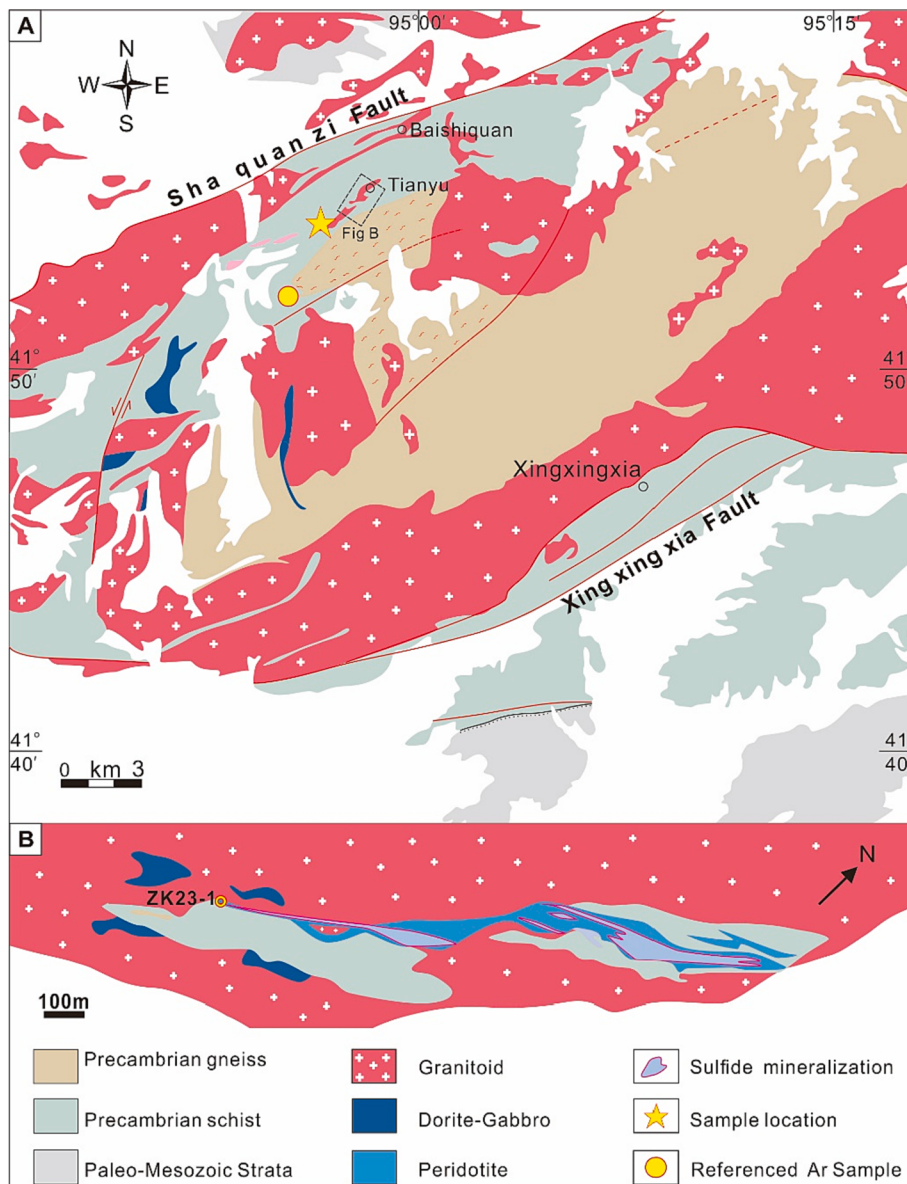


**Fig. 2.** (A) Simplified geological map of the study area; (B) geological map of the Tianyu Cu-Ni deposit (modified after Tang et al., 2009). The location of the boreholes is shown in Fig. 2B.

mainly comprises Silurian to Carboniferous sedimentary rocks (e.g., cherts, volcaniclastic rocks and turbidites) and ophiolitic mélange (Ao et al., 2010; Xiao et al., 2010; Wang et al., 2018).

The eastern Central Tianshan has a Precambrian basement that underwent greenschist to amphibolite facies metamorphism (Shu et al., 2003; He et al., 2015). Its Proterozoic basement rocks are mainly composed of gneisses, amphibolites, quartz schists and marbles (Fig. 1B and 2; Hu et al., 2010; Lei et al., 2013; Huang et al., 2015). These rocks are overlain by Cambrian to Permian volcanic rocks, limestones and siliciclastic (XBGMR, 1993; Xiao et al., 2004). Magmatic intrusions were emplaced from the Proterozoic to the Mesozoic in the Central Tianshan, with marked magmatic activity during the early Permian. Most of the unusual abundant mafic-ultramafic intrusions in the eastern Central Tianshan are relatively small in scale and were formed mainly during the early Permian (ca. 280 Ma; Wen et al., 2019).

The tectonic evolution of the Eastern Chinese Tianshan continued with new reactivation episodes during the Meso-Cenozoic as a response to accretions and collisions at the Eurasian margins. Due to this reactivation, its basement underwent extensive and diffuse intra-continental

deformation (e.g., Gillespie et al., 2017a; He et al., 2022a). In general, the Bogda - Harlik - Balikun mountain chain exhibits a thermo-tectonic history comparable to the other ranges of the Tianshan to the west (e.g., Jolivet et al., 2010; Glorie and De Grave, 2016), and widespread Jurassic to Cretaceous apparent AFT ages (Gillespie et al., 2017a; He et al., 2022a,b) are found.

## 2.2. Geology of the Tianyu deposit

The Tianyu Cu-Ni deposit contains estimated Ni metal reserves of ca. 22.3 thousand tons, and is currently being mined. The host lithologies of the deposit (i.e. the Tianyu intrusion) are lherzolite, olivine websterite and gabbro whose formation ages are constrained at ~ 280 Ma by SIMS zircon U-Pb dating (Tang et al., 2011). They intruded in late Paleozoic granites and Precambrian basements. Hydrothermal alteration is ubiquitous with olivine serpentinisation, orthopyroxene partially altered to talc and chlorite, and plagioclase partially altered to sericite, epidote, and albite. Sulfide mineralization occurs predominantly as disseminated and net-textured sulfides in the interstices of ultramafic rocks.

The Tianyu (mafic-ultramafic) intrusion is a dyke-like body with surface exposure of >1000 m in length and ~ 6–70 m in width (Fig. 2B), it strikes 49° and dips at 60–80° with vertical downward extension varying between ~ 250 to 350 m (Tang et al., 2012; Duan et al., 2017). Structurally, ~ENE trending faults and folds with ~ ENE-striking axial planes are well developed in the region (Fig. 2B), but no apparent deformation (e.g., displacement or folding) of the ore body is observed in the field.

### 3. Samples and methodology

To constrain the exhumation of the Tianyu Cu-Ni deposit, a total of five granitoid samples were taken at different depths from 32 m to 1198 m below the surface from the borehole ZK23-1 (N41°54'33.8" E 94°56'12.2") with a total depth of 1202.3 m. The lithologies occurring in the borehole section mainly include the undeformed late Carboniferous (~310 Ma) granodiorite and granite (Fig. 3A).

#### 3.1. Apatite fission track thermochronology

Low-temperature thermochronological analyses in this study were conducted at School of Earth Sciences, The University of Melbourne. Apatite grains were separated by conventional mineral separation techniques: using standard heavy liquid and magnetic separation procedures. Apatite grains were then mounted in epoxy resin, ground and polished. The polished mounts were etched in 5 M HNO<sub>3</sub> for 20 s at 20 °C to reveal fossil tracks. A Zeiss Axio Imager M1m microscope was used to select apatite grains for measurement with polished surfaces parallel to prismatic crystal faces and homogeneous track distributions. Then at a total magnification of  $\times 1000$ , a 3.2MP camera was used to capture a series of high-resolution digital images in both reflected and transmitted light (Gleadow et al., 2015). Uranium concentrations of corresponding grains were determined using an Agilent 7700 LA-ICP-MS coupled with a New Wave UP-213 laser over 25 s on selected grains (Li et al., 2019). Confined track length measurements were made on c-axis parallel grains as true 3D lengths using captured digital images. Where possible, >100 confined lengths were measured per sample. Etch pit diameters ( $D_{\text{par}}$ ) of all analyzed grains (age/length) were determined and used as kinetic parameters for thermal history modeling.

#### 3.2. Apatite and zircon (U-Th)/He dating

Inclusion-free apatite and zircon grains for (U-Th)/He analysis were handpicked from concentrated separates, based on their size, and euhedral crystal shape (where possible). Grain geometries were imaged microscopically and stored for applying the alpha-ejection age corrections (Farley et al., 1996). Apatite and zircon aliquots were loaded into platinum capsules and outgassed under vacuum at ~ 900 °C for 5 min and ~ 1300 °C for 15 min, respectively. The protocols of He analysis followed the established laboratory routine extraction. The <sup>4</sup>He abundances were determined as an isotope ratio using a pure <sup>3</sup>He spike that has been calibrated against an independent <sup>4</sup>He standard (House et al., 2000). The outgassed apatite grains were dissolved in HNO<sub>3</sub> and analysed for <sup>238</sup>U, <sup>235</sup>U, <sup>232</sup>Th, and <sup>147</sup>Sm. The degassed zircon grains were transferred to Parr bombs, where they were spiked with <sup>235</sup>U and <sup>230</sup>Th and digested at 240 °C for 40 h in HF. A second bombing in HCl for 24 h at 200 °C ensured the dissolution of fluoride salts. Zircon solutions were then dried down, dissolved in HNO<sub>3</sub>, and diluted in H<sub>2</sub>O to 5 % acidity for analysis of <sup>238</sup>U, <sup>235</sup>U, and <sup>232</sup>Th by solution ICP-MS (Gleadow et al., 2015).

#### 3.3. Thermal history modeling

Cooling histories of the Tianyu borehole samples were further derived by using the QTQt software package (version 5.6.0, Gallagher, 2012), this application performs inverse thermal modeling based upon

the Bayesian transdimensional Markov-Chain Monte-Carlo approach (Gallagher et al., 2009). The inverse scheme of this software is built to reconstruct the integrated thermal history of a set of borehole samples (with various depths), when all AFT ages, single-grain He data, track length distributions, kinetic parameters and other effective age constraints are taken into account.

In order to calculate proposed time-temperature paths of the Tianyu borehole section, we provided the program with spontaneous track density data, uranium concentration, and length frequency distributions of all the five granitoids. We use the multi-kinetic apatite fission track annealing model of Ketcham et al. (2007), with  $D_{\text{par}}$  serving as kinetic parameter (Ketcham et al., 1999). The radiation damage accumulation and annealing model (RDAAM) for helium diffusion in zircon (Guenther et al., 2013) were used to model He single-grain ages. An initial constraint at a temperature of 900 ± 50 °C was set at 280 ± 2 Ma based on the emplacement age of the pluton (Tang et al., 2011). We first ran 10,000 burn-in and 50,000 post-burn to find the appropriate search parameters, after that each 200,000 iterations were run as burn-in and post-burn-in iterations.

## 4. Analytical results

### 4.1. Apatite fission track data

All five granitoid samples from the borehole were analyzed using the AFT method. All samples yield Cretaceous central ages varying from ~ 99.5 to ~ 75.3 Ma (Table 1). More than twenty apatite grains were analyzed for each sample, and all the obtained ages pass the  $\chi^2$  test ( $P(\chi^2) > 5\%$ ) (Fig. 3), suggesting single age populations (Galbraith and Green, 1990). Four samples yield average  $D_{\text{par}}$  values of > 2  $\mu\text{m}$  (Table 1), indicative of relatively stronger resistance to annealing (e.g., Carlson et al., 1999). As to the track length data, all five samples yielded > 90 confined tracks (four of them > 100). Mean track lengths vary between ~ 13.9 and ~ 12.5  $\mu\text{m}$ . Especially for the top three samples, the track lengths are longer and concentrated between ~ 13.9–13  $\mu\text{m}$ , inferring less intense thermal annealing. Only the bottom sample 16WX-5–5 shows a much shorter mean track length (~12.5  $\mu\text{m}$ ) with a  $D_{\text{par}}$  value of ~ 1.6  $\mu\text{m}$ . The kinetic parameter  $D_{\text{par}}$  was used to determine fission-track annealing behaviour. Apatite crystals with higher  $D_{\text{par}}$  values are considered to exhibit stronger resistance to annealing, resulting in longer mean track length and vice versa. The small  $D_{\text{par}}$  value of 16WX-5–5 (Table 1) hence may account for relatively shorter confined track lengths there.

The age-depth relationships for these samples display a normal trend (i.e. deeper samples exhibit younger AFT central ages (Fig. 3B). And a remarkable apparent inflection point at ~ 95 Ma is also displayed in the AFT age-elevation plot, where the elevation is in the depth of ~ 674 m (Fig. 4). An estimated exhumation rate of ~ 81 m/Ma is obtained from the slope of the AFT central age-elevation plot above the inflection point. Between depths of ~ 674 m and ~ 1198 m (under the inflection point) AFT central ages decrease from ~ 95 to ~ 75 Ma, and the exhumation rate decreases to ~ 26 m/Ma, suggesting the onset of much slower basement cooling.

### 4.2. Zircon and apatite (U-Th)/He data

For (U-Th)/He analysis, we acquired ZHe ages of two samples and AHe ages of four samples (Table 2).

Six single aliquot zircon ages were obtained for samples 16WX-5-3 and 5-5, both of which show over-dispersed age datasets with dispersion that is greater than it would be expected from analytical uncertainty alone (Table 2). There may be several explanations for intrasample variations (Reiners and Farley, 2001; Fitzgerald et al., 2006). The single-grain ZHe ages do not show clear relationships with effective Uranium (eU) and grain size (Fig. 5), indicating that radiation damage effects and variation of grain size are less likely to affect the age distribution.

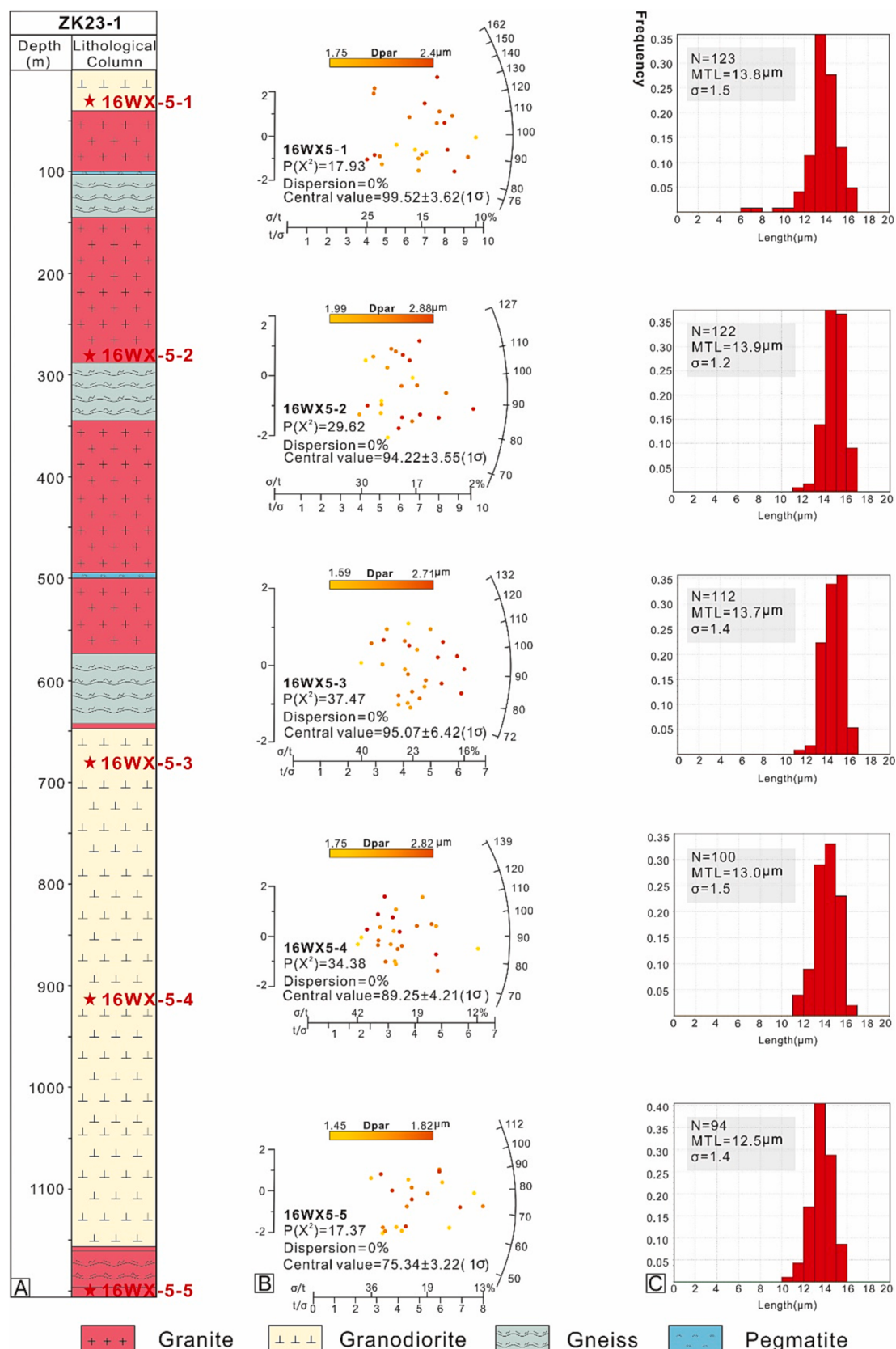


**Fig. 3.** (A) The Sample depths are shown on the lithological column of ZK23-1 borehole. (B) Apatite fission track radial plots. The color of single-grain AFT ages correspond to their  $D_{\text{par}}$  value (in  $\mu\text{m}$ ). Dispersion = age-dispersion value as a percentage;  $P(\chi^2)$  = chi-squared probability; (C) corresponding confined track histograms. N = the number of lengths measured.

**Table 1**

Apatite fission track data for Paleozoic basement rocks from the borehole ZK23-1.

Sample No.	depth [m]	No. of grains	$N_s$	$\rho_s (10^5 \text{ cm}^{-2})$	$^{238}\text{U}$ (ppm)	$D_{\text{par}}$ ( $\mu\text{m}$ )	$P(\chi^2)$ (%)	Central age (Ma $\pm$ 1 s.e.)	$N_{\text{length}}$	Mean track length ( $\mu\text{m}$ )	Standard Deviation ( $\mu\text{m}$ )
16WX5-1	-32	23	2426	12.56	27.99	2.08	17.93	99.5 $\pm$ 3.6	123	13.8	1.5
16WX5-2	-298	25	1208	4.42	9.26	2.42	29.62	94.2 $\pm$ 3.6	122	13.9	1.2
16WX5-3	-674	21	450	3.37	8.15	2.09	37.47	95.1 $\pm$ 6.4	112	13.7	1.4
16WX5-4	-903	22	591	3.36	8.09	2.13	34.38	89.2 $\pm$ 4.2	100	13.0	1.5
16WX5-5	-1198	21	1031	8.80	25.92	1.62	17.37	75.3 $\pm$ 3.2	94	12.5	1.4

$N_s$  = number of spontaneous tracks counted;  $\rho_s$  = spontaneous track density;  $D_{\text{par}}$  = long axis of track etch pit;  $N_{\text{length}}$  = number of lengths measured.

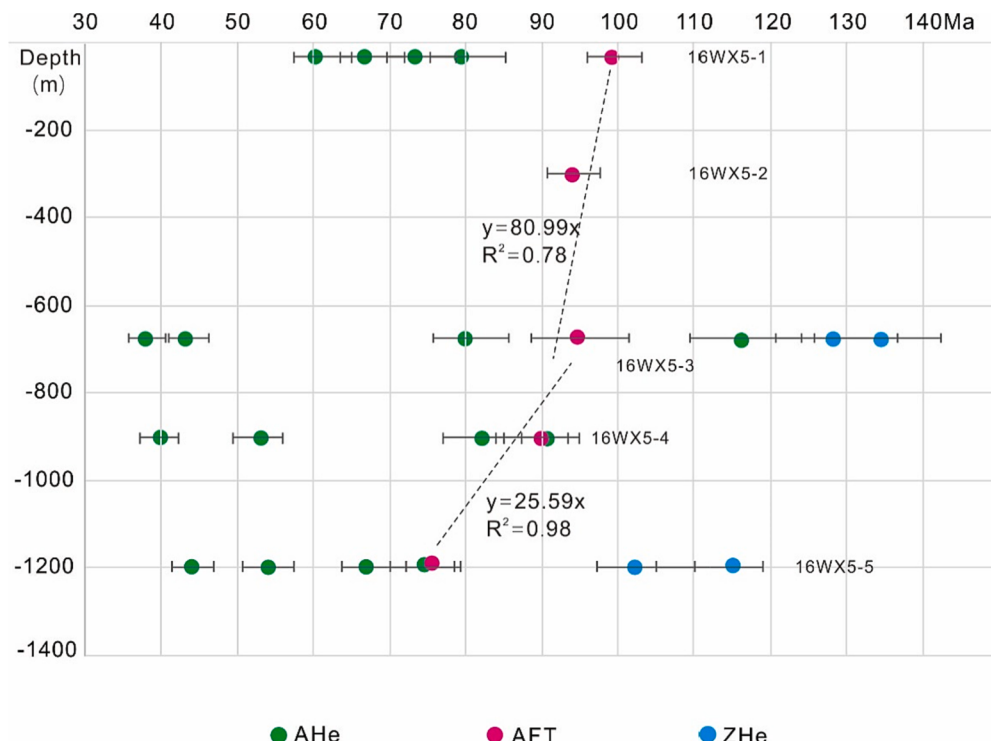


Fig. 4. Age-depth plots of borehole sample. The different depths in the y axis represent the different samples.

Considering that the analyzed zircon grains are euhedral, displaying two terminations, some other potential effects such as U-Th-zoning or grain breakage may be responsible for the much younger single grain ages. After discounting the two grains with ZHe ages younger than their respective AFT ages (~74.9 Ma, 16WX5-3; ~70.0 Ma, 16WX5-5), the remaining dates give ZHe ages of ~134.0–128.6 Ma for sample 16WX5-3 and ~112.0–103.7 Ma for 16WX5-5, which were incorporated individually into the integrated QTQt modeling.

Apatite (U-Th)/He analyses were carried out on sixteen grains from four samples (except for 16WX5-2). Among them, three samples (16WX5-3, 5–4 and 5–5) yield clear over-dispersed (U-Th)/He results (Table 2). The AHe intrasample age data dispersion can also be related to similar factors as for the ZHe age dispersion outlined above. The ages are plotted as a function of eU in Fig. 5. It is strongly suggested that over-dispersed AHe ages (>20 %, one standard deviation) samples without age-eU or age-grain size correlations should not be used for in-depth interpretations (Flowers and Kelley, 2011). In this regard, only AHe ages of sample 16WX5-1 is withheld in the following discussion.

#### 4.3. Thermal history modeling results

The He dispersion in apatite can be influenced by grain fragmentation variation with terminations number (0 T, 1 T or 2 T). One termination (1 T) fragments usually yield older or younger ages than the whole grain age, while no termination (0 T) grains would most likely

yield older ages (Beucher et al., 2013). Since all the analyzed apatite grains only exhibit one or zero termination (T) geometry (listed in Table 2), we did not incorporate the AHe data into the thermal history modeling, as this would lead to erroneous  $F_T$  correction and hence AHe ages. Meanwhile, due to He age dispersion within the sample and our inability to assess the influence of factors that may be involved, in order to ensure the reliability of the thermal history modeling output, less weighting was given to the He data for modeling. First, only AFT data was used to establish a baseline from which different model versions were built progressively. The model with only AFT ages shows a pronounced cooling episode between ~100 and ~90 Ma (Fig. 6A). One benefit of choosing QTQt in this study is that He data can be resampled from their age. Some of the undefined uncertainty can be accounted for by regarding the He ages as less precise while still honoring the observed ages (Gallagher, 2012). Therefore, the individual grain age, rather than the mean He age, was progressively incorporated into the model to provide additional constraints. The addition of ZHe data to our models preferred the AFT model that the cooling may have commenced a little earlier, around 110 Ma with the estimated rate of 5 °C/Ma (Fig. 6B).

The integrated thermal history modeling for the Tianyu drilling section, constrained by AFT and ZHe results obtained in this study as input, as well as additional published zircon U-Pb (Tang et al., 2011) and mica Ar-Ar dates (Wang et al., 2022), reveals a multi-stage cooling history (Fig. 6C). The first stage involves cooling from the early Permian formation of the pluton to ~320 °C in the middle Permian as indicated

**Table 2**  
Single apatite and Zircon grain (U-Th)/He data of borehole ZK23-1.

Sample No.	<sup>4</sup> He gas ncc	Mass (mg)	<sup>a</sup> Mean FT	U ppm	Th ppm	Sm ppm	Th/U	<sup>b</sup> [eU] ppm	Uncorrected Age (Ma)	Corrected Age (Ma)	Error ± 1 s (Ma)	Grain length (mm)	Grain width (mm)	Grain morphology
<b>Apatite</b>														
16WX5-1	6.57	0.02	0.85	31.70	22.50	28.40	0.71	36.99	68.03	80.27	4.98	288.73	171.49	0 T
16WX5-1	2.31	0.01	0.82	25.10	12.30	33.60	0.49	27.99	50.23	61.24	3.80	254.22	145.08	0 T
16WX5-1	3.44	0.01	0.83	35.80	17.80	61.90	0.50	39.98	61.57	74.18	4.60	268.18	159.91	1 T
16WX5-1	1.61	0.01	0.80	18.00	23.30	51.70	1.29	23.48	54.36	67.69	4.20	209.32	139.99	0 T
16WX5-3	0.07	0.00	0.73	2.70	8.40	35.90	3.15	4.67	27.85	38.18	2.37	157.84	106.03	0 T
16WX5-3	0.06	0.01	0.76	1.40	3.60	15.30	2.64	2.25	33.19	43.61	2.70	177.65	120.57	0 T
16WX5-3	0.26	0.01	0.74	3.50	13.80	53.50	3.90	6.74	59.75	80.71	5.00	245.19	108.94	1 T
16WX5-3	0.46	0.01	0.78	3.10	9.80	21.00	3.14	5.40	91.02	116.74	7.24	266.21	127.29	1 T
16WX5-4	0.16	0.00	0.70	3.70	10.10	60.50	2.72	6.07	62.66	89.42	5.54	167.03	89.83	0 T
16WX5-4	1.52	0.00	0.71	48.10	72.90	138.00	1.51	65.23	58.35	82.20	5.10	123.34	102.34	0 T
16WX5-4	0.13	0.01	0.78	1.80	4.30	51.90	2.42	2.81	41.06	52.72	3.27	256.50	117.39	0 T
16WX5-4	0.25	0.00	0.73	13.10	13.30	36.50	1.02	16.23	29.02	39.76	2.47	196.19	93.61	0 T
16WX5-5	0.25	0.01	0.80	4.50	1.50	16.00	0.34	4.85	43.31	53.98	3.35	239.87	125.70	0 T
16WX5-5	0.47	0.01	0.81	9.60	3.60	83.60	0.38	10.45	35.79	44.24	2.74	240.86	130.06	0 T
16WX5-5	1.71	0.01	0.78	26.30	10.20	135.20	0.39	28.70	58.34	74.64	4.63	280.46	108.71	0 T
16WX5-5	0.35	0.01	0.76	10.10	3.90	98.70	0.39	11.02	51.37	67.94	4.21	197.48	100.86	0 T
<b>Zircon</b>														
16WX5-3	11.14	0.00	0.68	291.42	169.83	*	0.58	331.33	87.38	128.59	7.97	148.50	67.91	2 T
16WX5-3	35.15	0.01	0.77	323.54	414.04	*	1.28	420.84	102.87	133.96	8.31	187.69	96.27	2 T
16WX5-3	1.77	0.00	0.70	70.30	61.71	*	0.88	84.81	52.20	74.90	4.64	141.02	75.40	2 T
16WX5-5	101.65	0.01	0.79	1216.98	103.65	*	0.09	1241.34	54.83	68.98	4.28	316.96	91.26	2 T
16WX5-5	135.94	0.01	0.78	1888.92	226.19	*	0.12	1942.07	81.35	103.68	6.43	200.31	94.93	2 T
16WX5-5	60.25	0.00	0.74	977.54	282.07	*	0.29	1043.83	83.36	111.97	6.94	212.94	75.59	2 T

<sup>a</sup>F<sub>T</sub> is the a-ejection correction after Farley et al. (1996).

<sup>b</sup>Effective uranium concentration (U ppm + 0.235 Th ppm).

<sup>c</sup>Grain morphology – 0 T = no terminations, 1 T = one termination, 2 T = 2 terminations.

by muscovite <sup>40</sup>Ar/<sup>39</sup>Ar data. This gives an average cooling rate of ~26 °C/Ma in this period. This initial cooling phase was followed by a late Permian-Early Triassic moderate cooling (~3.5 °C/Ma) episode as constrained by both muscovite and biotite <sup>40</sup>Ar/<sup>39</sup>Ar data. Thereafter, the studied rock section underwent protracted slow exhumation throughout the early-middle Mesozoic, which gradually brought the rocks to the zircon HePRZ (i.e. ~180 ± 20 °C) (Reiners et al., 2004). Subsequently, renewed moderate denudation occurred at the Early to Late Cretaceous (~115–85 Ma). During this phase, more rapid cooling from ~200–170 °C at ~115 Ma to ~90–60 °C at ~85 Ma transpired. Here, the single-grain AHe ages (~80–61 Ma) for the sample 16WX5-1 are in good agreement with the integrated modeling results, if we assume an AHe closure temperature of ~75–50 °C (Farley, 2000). Since the Late Cretaceous, all the samples in the section experienced relatively slow cooling until the present.

## 5. Discussion

### 5.1. Cooling and exhumation history of the Tianyu Cu-Ni deposit

Integrated thermal history modeling results indicate that the first rapid basement cooling in the study area occurred during ~280–260 Ma. The published 280 ± 2 Ma zircon U-Pb age (Tang et al., 2011) represents the crystallization age of the host rock of the Tianyu deposit. A previously obtained Re-Os age (835 ± 210 Ma) of the sulfide ores in the Tianyu deposit is much older than that of the nearby Baishiquan deposits (286 ± 14 Ma) and seems rather imprecise (Wang et al., 2007). The narrow Re-Os age range of ~298–270 Ma for other Cu-Ni deposits in the eastern Tianshan (Han et al., 2010b) indicates that mineralization is closely related to the emplacement of Permian igneous complexes. Based on zircon U-Pb ages of the host rocks, we consider that the Tianyu ore body may have rapidly cooled through the ~550–500 °C isotherm

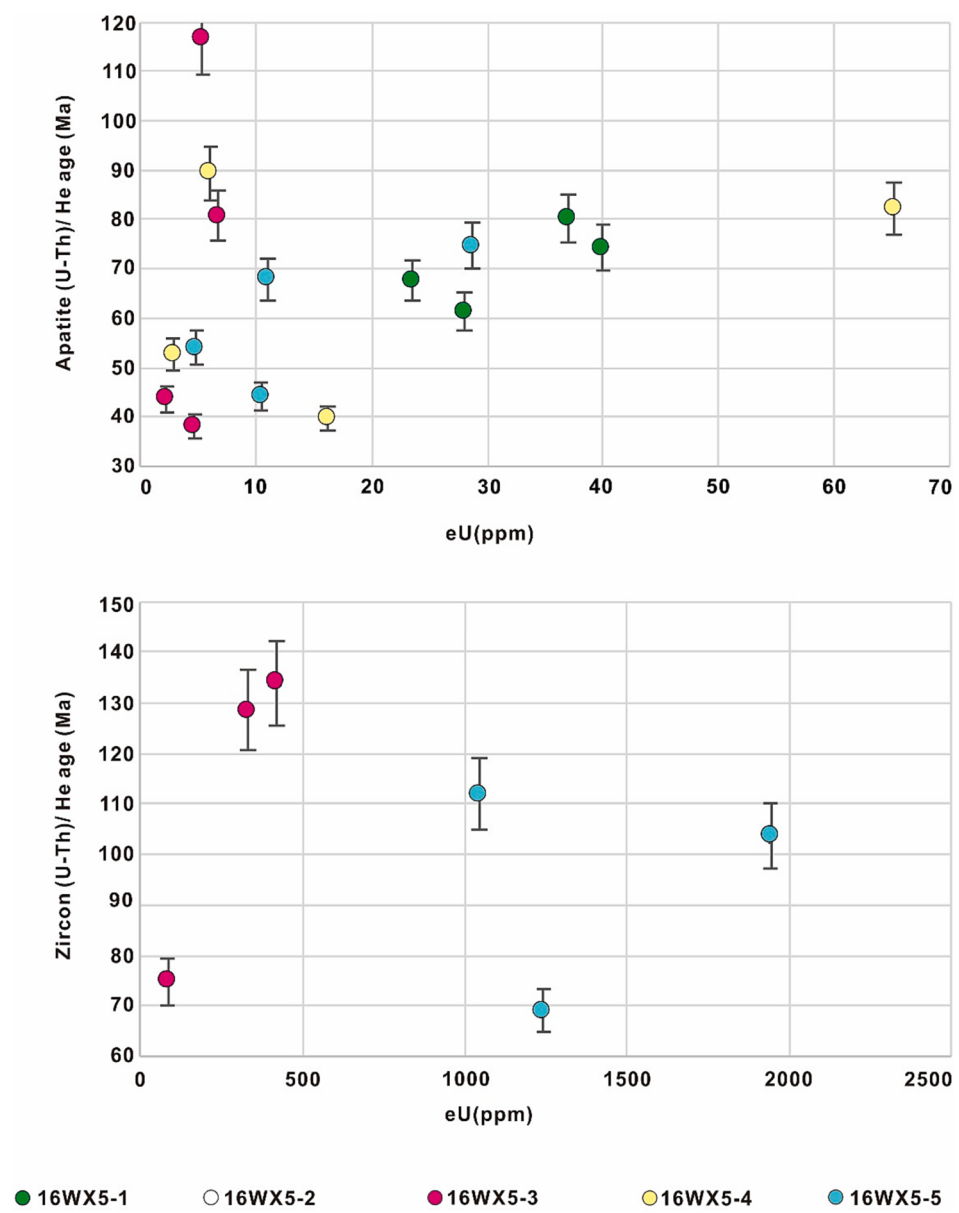


Fig. 5. AHe and ZHe age as a function of effective uranium concentration (eU ppm).

(estimated closure temperature of the molybdenite Re-Os system; Suzuki et al., 1996) and experienced hydrothermal alteration soon after its emplacement. We hence interpret the ~ 280–260 Ma fast cooling as post-magmatic cooling and thermal equilibration after the emplacement (Fig. 7A).

The subsequent ~ 260–240 Ma moderate cooling recognized in our thermal history model was widespread along major shear zones, as shown by available  $^{40}\text{Ar}/^{39}\text{Ar}$  cooling ages from several areas in the Tianshan (Dumitru et al., 2001). Although there are different views on the triggering factor of this late Permian-Early Triassic event, such as the closure of the Paleo-Asian Ocean (Xiao et al., 2009), large-scale block rotation and reorganization (Allen et al., 2006) and intra-continental tectonic adjustment (Shu et al., 1999), it is widely accepted that the late Paleozoic-earliest Mesozoic deformation of the Tianshan belt was dominated by transcurrent tectonics (He et al., 2021a). We therefore propose that the study area experienced regional tectonic activity controlled by intense strike-slip fault movements during this time span (~260–240 Ma; Fig. 7B), resulting in basement rock denudation and consequential moderate cooling as evidenced in our thermal history model.

This moderate cooling was followed by a widespread relief lowering process (Hao et al., 2006) that marked the end of the transcurrent tectonism and the development of an early Mesozoic flat topography in Central Asia (e.g., Jolivet et al., 2013). A widespread coal-bearing sediment sequence and peneplains developed over most Central Asia by the Middle Jurassic, probably extending from the northern Tibet to SE Siberia (Vassallo et al., 2007). AFT track data obtained from the adjacent Chinese Central Tianshan (Gangou) show a cooling stagnation from the Triassic to Middle Jurassic (He et al., 2021b). More recently, He et al. (2022c) found that the Bogda Shan to the north underwent similar prolonged slow to slightly moderate cooling during most of the Mesozoic. This prolonged cooling period from the Middle Triassic to Late Cretaceous corresponds to a very low erosion rate of ~ 4–7 m/Ma (Jolivet et al., 2010).

Following the early Mesozoic protracted slow cooling, the integrated inverse thermal history models reveal a distinct signal of Cretaceous cooling, with ~ 100 °C cooling occurring between ~ 115 and ~ 85 Ma (Fig. 6 and 7C-D). Many of the previous studies relate (Early) Cretaceous cooling in Central Asia to the collision-accretion of the Lhasa and Qiangtang micro-continents (e.g., Yin and Harrison, 2000) along the

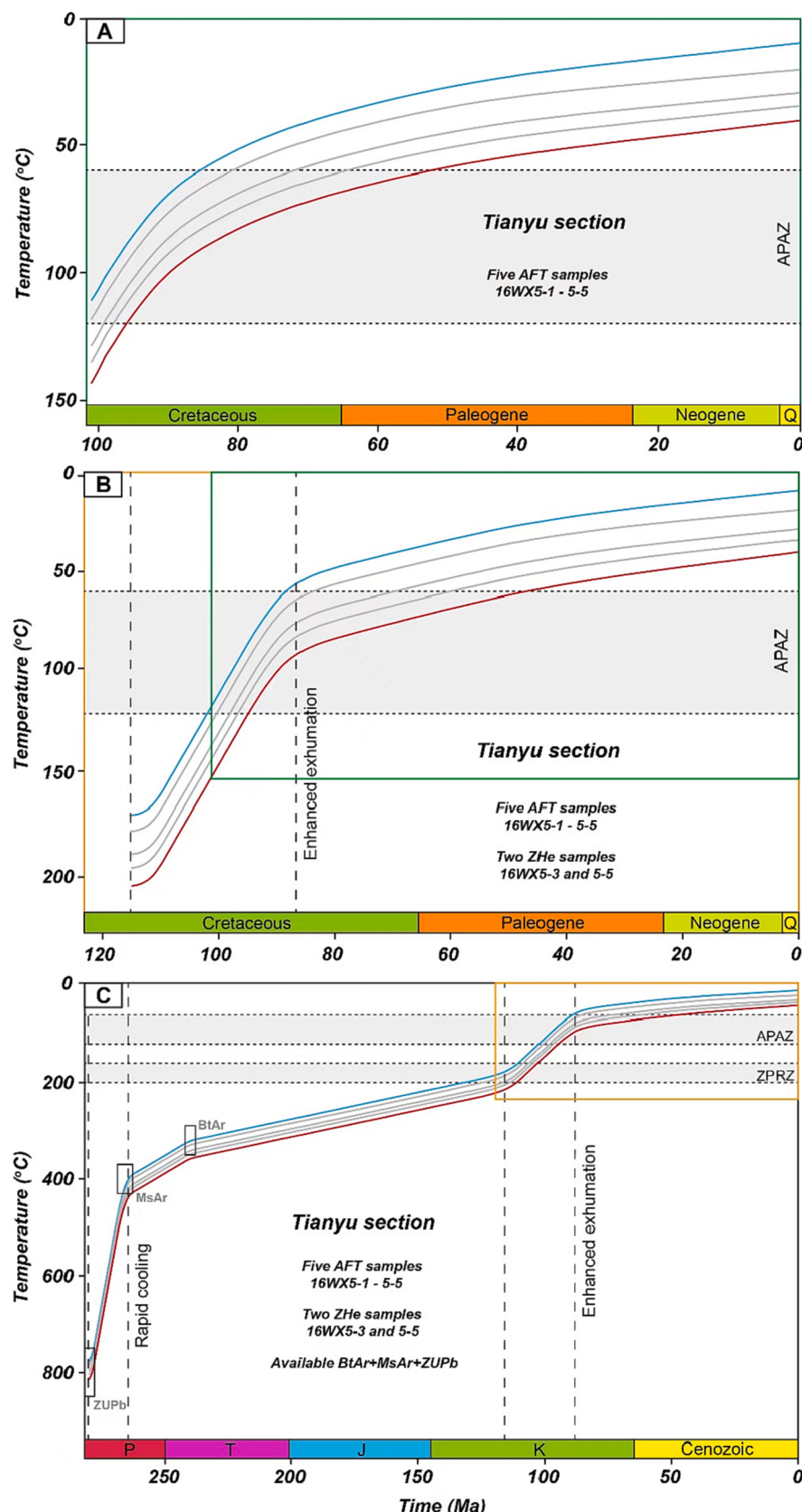


**Fig. 6.** Integrated QTQt thermal history of the Tianyu ore deposit based on AFT only (A); ZHe & AFT (B); and ZUPb, MsAr, BtAr, ZHe and AFT (C), showing a pronounced mid-Cretaceous cooling episode between ~115 and ~85 Ma. (see section 4.4 for discussion).

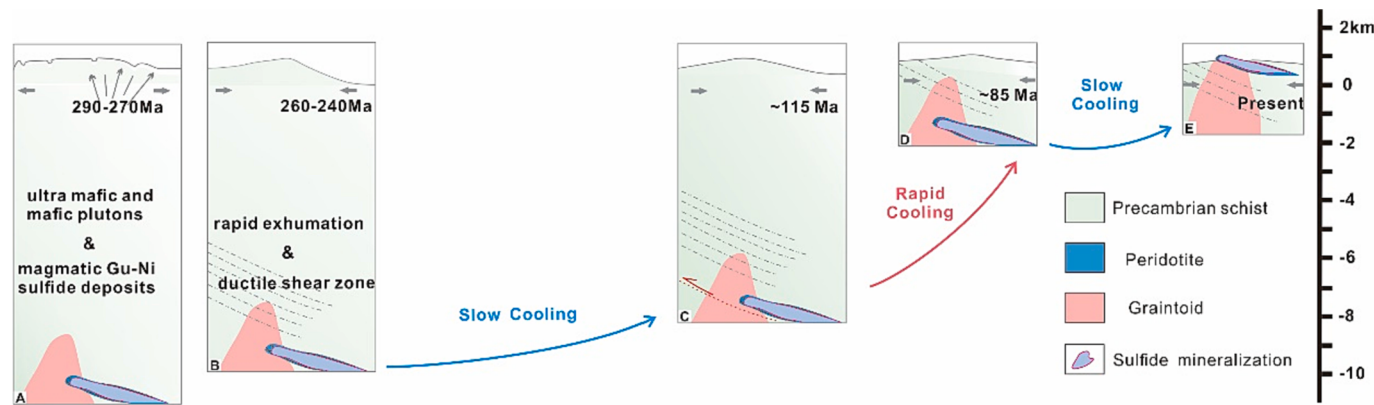


**Fig. 7.** Schematic diagrams show the uplift and denudation history of the Tianyu deposit. See text for details.

southern Eurasian margin. It is now generally accepted that the ‘hard’ collision between the Lhasa and Qiangtang blocks initiated at ~130–120 Ma (e.g., Li et al., 2016; Kapp and DeCelles, 2019). In such a compressional regime, far-field effects usually result in surface uplift, and an erosional procedure is necessary to create denudation when thermochronological clocks re-commence. A distinct time-lag (up to several million years) is therefore often observed between the timing of a (distant continental) collision and the onset of intra-continental cooling (e.g., Glorie and De Grave, 2016). In this regard, the ~115–85 Ma cooling pulse spatio-temporally fits well with the possible far-field effects generated by the Lhasa-Qiangtang collision.

The analyzed borehole samples all show very limited cooling since the Late Cretaceous. The upper three samples in the section have cooled out of the APAZ before the Cenozoic (Fig. 6C), suggesting that less than ~1–1.5 km exhumation has occurred during the Cenozoic (Fig. 7E). This is probably because the Cenozoic tectonic uplift and surface erosion (in a semi-arid to arid climate) in the study area were not intensive enough to exhume deeper crustal levels that would, after thermal relaxation of the crustal isotherms, induce cooling of the basement with associated younger thermochronological ages.

## 5.2. Regional comparisons

The newly-obtained thermochronological results in this study are generally in agreement with earlier work on basement rocks in the Chinese Tianshan and adjacent areas. A large set of Permian-Early Triassic cooling ages and relevant structural data have been reported from several major shear zones in the Eastern Tianshan, indicative of coeval intensive intra-continental deformation. Along the Aqikekuduke-Weiye fault (eastern segment of the Main Tianshan shear zone), muscovite from a mylonitic granite (near Gangou) yield  $^{40}\text{Ar}/^{39}\text{Ar}$  plateau and isochronal ages of  $269.1 \pm 5.4$  and  $268.8 \pm 5.4$  Ma, respectively (Shu et al., 2002). In the Kumishi fault, a syn-kinematic potassic granite displaying strong mylonitic foliations yielded a zircon U-Pb age of ~252 Ma (Wang et al., 2009). Muscovite and biotite  $^{40}\text{Ar}/^{39}\text{Ar}$  results, together with zircon U-Pb ages of syn-kinematic plutons demonstrate that sinistral motion along the Xingxingxia shear zone initiated at ~240–235 Ma. Similar  $^{40}\text{Ar}/^{39}\text{Ar}$  plateau ages (~260–240 Ma) were also obtained on samples that are in the immediate vicinity of the easternmost Aqikekuduke-Weiye fault (Wang et al., 2022) (Fig. 2A), and identical (~260–240 Ma) enhanced basement cooling due to exhumation along strike-slip faults is shown by the inverse thermal history models reported here.

Cretaceous basement cooling has been widely recognized throughout the Tianshan belt from west to east: in the Talas-Fergana region (Nachtergael et al., 2018), the Issyk-Kul and Song-Kul regions (De Grave et al., 2011, 2013) of the Kyrgyz Tianshan; and in the *trans*-Ili-Balkhash (De Pelsmaeker et al., 2015) in Kazakhstan. For the Chinese

Tianshan, based on new data presented here and a synthesis of the literature, basement cooling in the Cretaceous has also been recognized, with the age and magnitude being spatially variable (Fig. 8).

Differential exhumation patterns occur along the E-W-trending Main Tianshan shear zone (MTSZ), with limited cooling in the western-central part and enhanced basement cooling in its eastern part since the late Paleozoic.

Permian to Early Cretaceous AFT ages and associated thermal history models reveal that the basement cooling of the Yili block only underwent slow to moderate cooling in the Cretaceous and this large area seems to have experienced a rather small amount of exhumation (<~2–4 km) since the early Mesozoic (Fig. 8A; He et al., 2022c). Only small-scale brittle faults that are not directly linked with the regional major faults controlled localized enhanced denudation (Wang et al., 2018, 2021; Glorie et al., 2019).

In the western Central Tianshan, although a few young Cenozoic cooling ages were recognized along the Du-Ku road transect, thermal history models of the majority of samples there indicated an episode of slow basement cooling in the Middle Jurassic-Cretaceous (Fig. 8B; Dumitru et al., 2001; Yin et al., 2018). Data from samples taken from the vicinity of the Main Tianshan shear zone in the Gangou and Alagou areas (Fig. 8C), also confirm that less exhumation since 150 Ma transpired (He et al., 2021b).

While in the central part of the Central Tianshan, low-temperature thermochronological data are still rather limited due to the poor investigations. The Aqikekuduke fault is the eastward extension of the MTSZ, and represents a clear tectonic boundary between the Central and North Tianshan (Shu et al., 2002). Samples from the western segment of the Aqikekuduke fault yield older, Late Triassic ZHe ages (210–230 Ma) and Late Jurassic AFT and AHe ages (130–150 Ma) (Fig. 8D). Associated thermal history models revealed slow basement cooling since ~218 Ma, with slower cooling rates since 150 Ma, indicative of limited exhumation in the Cretaceous (Sun et al., 2021).

Along the eastern segment of the Aqikekuduke fault, as for actually the whole easternmost Tianshan, Meso-Cenozoic reactivation is much stronger, particularly during the Cretaceous. From a north-south transect across the easternmost Tianshan, Cretaceous basement cooling and exhumation is manifested along several major faults, including the Harlik, Dacaotan, Aqikekuduke and Xingxingxia faults. AFT age distribution there corresponds to differential fault-block exhumation patterns with the youngest ages occurring near the faults. In the north of the Balikun basin (Fig. 8E), Chen et al. (2020) identified a basement cooling phase at ~113–92 Ma with an estimated exhumation rate of ~58 m/Ma in the Moqingwula (also called Daheishan) range. Similarly, Gillespie et al. (2017a) obtained decreasing cooling ages from east to west along the eastern Daheishan. The exhumation of this massif is controlled by a pair of outward directed thrust faults. A cooling pulse is documented since ~80 Ma (Fig. 8F). In the Bogda-Harlik Arc, He et al. (2022a)

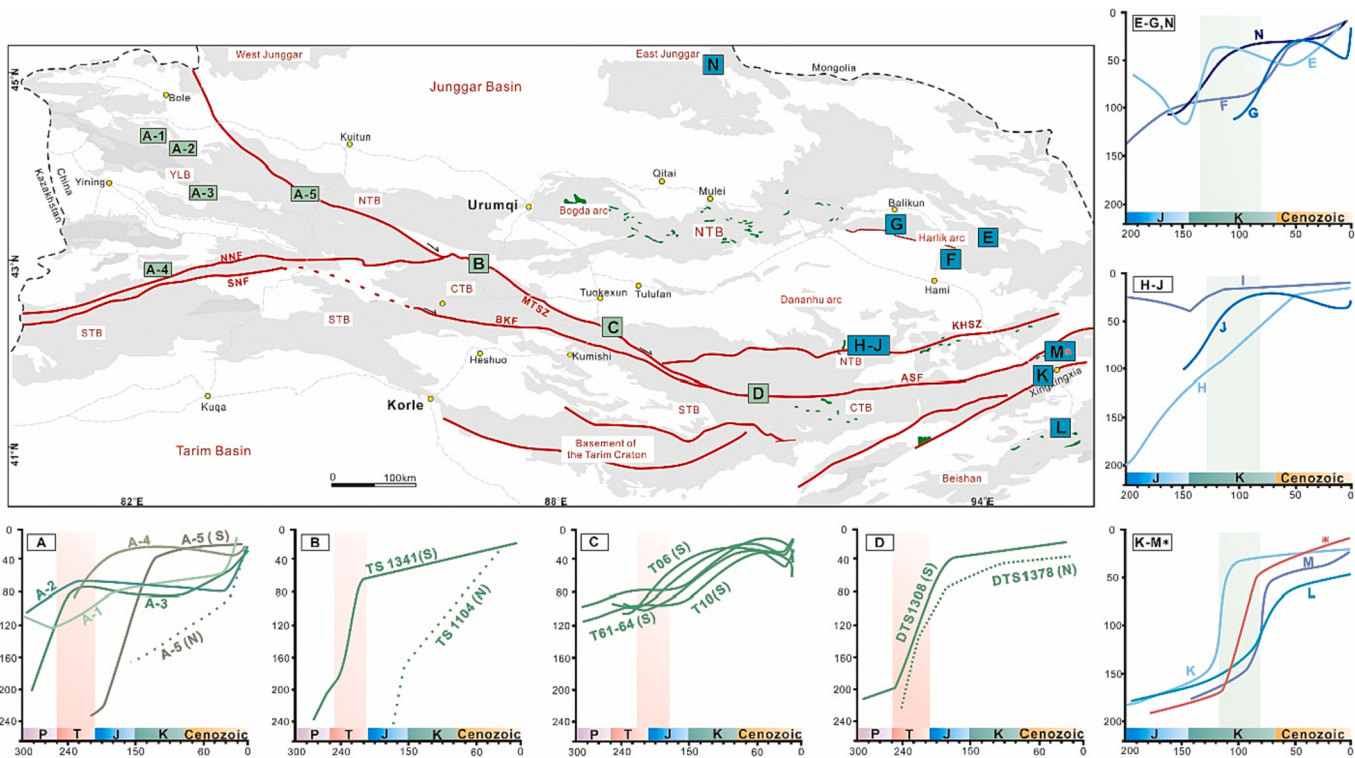


**Fig. 8.** Comparison of Cretaceous thermal histories with adjacent regions. The green bar represents the Cretaceous accelerated cooling; A-1 from Wang et al. (2021); A-2 Wang et al. (2018); A-3 Glorie et al. (2019); A-4 from He et al. (2022c); A-5 from Dumitru et al. (2001); Yin et al. (2018); B from Yin et al. (2018); C from He et al. (2021b); D from Sun et al. (2021); E from Chen et al. (2020); F Gillespie et al. (2017); G from He et al. (2022a); H from Yin et al. (2019); I from Gong et al. (2021); J from He et al. (2022a); K and L from Gillespie et al. (2017b); M from Wang et al. (2022); N from He et al. (2022a). (For interpretation of the references to color in this figure legend, the reader is referred to the web version of this article.)

identified a moderate basement cooling from the Cretaceous to Eocene (105–45 Ma), with a total cooling of >80 °C (Fig. 8G).

Available thermochronological data from the Tuwu-Yandong porphyry copper deposits (along the Dacaotan fault), located in the north of the Tianyu deposit, seem controversial. Yin et al. (2019) reported Early Cretaceous to Paleocene cooling with a cooling rate of ~2 °C/Ma and an associated rock exhumation rate of ~64 m/Ma (Fig. 8H). Whereas Gong et al. (2021) reported a lower exhumation rate of 22 ± 9 m/Ma with a total magnitude of 1.4 ± 0.6 km between ~165 and ~100 Ma (Fig. 8I), and argued for a localized fault control on different exhumation rates between the northern and southern parts of the ore field. In addition, also from this domain, He et al. (2022a) reported a similar moderate cooling episode (~1.5–1 °C/Ma) (through the APAZ) during ~150–120 Ma (Fig. 8J). To the south of Tianyu, samples with younger apparent AFT and AHe ages (around 100 Ma) from near the Xingxingxia fault (Fig. 8K) reveal that the eastern Central Tianshan basement likely experienced relatively rapid cooling at ~110–100 Ma with more intensive exhumation in the fault axis (Gillespie et al., 2017a). In other areas of the eastern Central Tianshan, AFT data also suggest regional Late Cretaceous accelerated cooling (~92.5 to 70.5 Ma) (Fig. 8M; Wang et al., 2022). When focusing further to the south (Fig. 8L), the Beishan area records similar Cretaceous AFT ages ranging from ~150 to ~108 Ma (Gillespie et al., 2017b). Therefore, all these published results have confirmed widespread basement exhumation and its consequential cooling in the Eastern Chinese Tianshan since the Early Cretaceous. Further, in the southern part of the East Junggar (the Yemaquan arc), Cretaceous accelerated basement cooling is also well documented (Fig. 8N; He et al., 2022a). Recognized cooling episodes there lasted until the Late Cretaceous and are highly comparable with the thermal history of the Eastern Chinese Tianshan.

It is worth mentioning that some authors argue for slow erosion rates and very limited tectonic uplift in the central and western Chinese

Tianshan during the latest Cretaceous-Eocene, and paleo-topography was associated with very low subsidence rates in the surrounding basins (e.g., Jolivet et al., 2010, 2018). Our thermal history models from the easternmost Tianshan basement rocks indeed generally display decreasing cooling rates or cooling stagnation during this time-span (Fig. 6). Therefore, our data are also in agreement with these observations derived from field and remote sensing data, and suggest that a large area of the Chinese Tianshan was less tectonically active in the latest Cretaceous-Eocene. On the other hand, no Cenozoic ages nor Cenozoic signals in the thermal history models were found in this study, suggesting that the Cenozoic exhumation was limited (less than ~2 km). This, along with other recent low-temperature thermochronological data (He, 2022), corroborate that recent (Cenozoic) deformation occurring in the Tianshan interior is comparably weak and has not resulted in significant rock exhumation (e.g., Avouac et al., 1993; Yin et al., 1998; Burchfiel et al., 1999; He et al., 2022b). This is in accordance with the preservation of numerous planation surfaces in the nearby Bodga - Balikun - Harlik mountain chain as well (Cunningham et al., 2003; Morin et al., 2019 ; He et al., 2022b).

### 5.3. Implications for prospecting in the Eastern Chinese Tianshan

The current exposure of the ore deposits is achieved through post-mineralization exhumation, which is usually controlled by regional fault activity (e.g., McInnes et al., 2005; Kesler and Wilkinson, 2006). In case of the Tianshan belt, determining the ‘magnitude’ of fault reactivation revealed by (low-temperature) thermochronological data could provide critical insights for exploration. So far, a number of basement samples from the vicinity of several large-scale Paleozoic strike-slip faults along the Chinese Tianshan belt have been analyzed by low-temperature thermochronological methods.

In our study area, Permian-Early Triassic ductile shearing of the

Aqikekuduke and Xingxingxia faults resulted in contemporaneous enhanced rock cooling and exhumation. After regional uniform Triassic cooling as mentioned above, most areas have undergone slow basement cooling or even a brief Jurassic reheating, i.e. reburial episode that eventually facilitated the preservation of porphyry systems and epithermal deposits (e.g., Wang et al., 2018, 2021). Conversely, detrital zircons U-Pb data from the surrounding basins reveal that the Central Tianshan was the main sedimentary source area to these basins during the Meso-Cenozoic (Fang et al., 2019a), indicating that the Central Tianshan was actively being eroded and exhumed at that time. This moderate to rapid cooling can be interpreted in terms of deeper basement exhumation during the Cretaceous, and is vital for exposing massive deep-seated deposits in the Eastern Tianshan. The Tianyu and other magmatic Cu-Ni sulfide ore deposits mineralized in middle crust (~11–15 km depth), with estimated temperature-pressure conditions of ~940–1080 °C, and ~250–450 MPa, respectively (Fang et al., 2019b). These deposits were exhumed close to the surface due to the Cretaceous (~115–85 Ma) reactivation of the Aqikekuduke fault (Fig. 7). The integrated thermal history models suggest that the most extensive exhumation (initial thermal equilibrium after its formation is excluded) of the Tianyu host rocks occurred in the Mesozoic, ultimately leading to the exposure of these massive deep-seated deposits.

On the other hand, for the Eastern Chinese Tianshan, no evidence was found for intense exhumation in response to the Cenozoic India-Asia collision. It is evident that large areas of the Eastern Tianshan (i.e. south of the Turpan-Hami basin) exhibit low elevations and relatively flat topography. This latter observation, together with low-temperature thermochronological evidence (e.g., Gillespie et al., 2017a, 2017b; Yin et al., 2019; Gong et al., 2021; He et al., 2022a, 2022b; this study), suggests that tectonic units such as the southern North Tianshan and Central Tianshan acted as relatively rigid blocks without significant reactivation of local structures and hence little or no basement cooling during the Cenozoic.

In general, the large-scale inherited structures were differentially reactivated in the intra-continental evolutionary stage. For the Eastern Tianshan and the adjacent areas, more significant fault reactivation occurred during the Mesozoic, with limited exhumation in the Cenozoic. It is noted that the Meso-Cenozoic thermal history of the Harlik mountain range is in fact highly comparable with that of the ‘flat areas’ in the Eastern Chinese Tianshan (e.g., He et al., 2022a). This suggests that part of the Harlik mountain (arc) may also have good potential for the preservation of the Paleozoic ore deposits like the eastern Central Tianshan to the south, due to a similar degree of exhumation.

## 6. Conclusion

Inverse thermal history modeling results based on our new borehole AFT and (U-Th)/He data, together with published datasets provide better constraints both on the thermal evolution of the Tianyu Cu-Ni ore deposits and, on a broader scale, on the intra-continental deformation history of the eastern Central Tianshan during the Mesozoic-Cenozoic. Our results indicate a four-stage post-Paleozoic cooling history accompanying and governing the formation, exposure and preservation of the ore deposit. An initial rapid cooling in the late Permian was the result of post-magmatic thermal equilibration, which was followed by moderate basement cooling and exhumation transpiring in a coeval transcurrent deformation pulse. Subsequent protracted slow regional basement cooling occurred during most of the early-middle Mesozoic. It was interrupted by an enhanced cooling episode (~3–4 °C/Ma) in the mid-Cretaceous (~115–85 Ma), triggered by fault reactivation as a response to far-field effects of the Lhasa-Qiangtang collision. Since then, the region was again dominated by very slow basement cooling rates throughout the Late Cretaceous-Cenozoic.

The complex and long-lasting post-mineralization exhumation plays an essential role in exposing deep crustal metallogenic systems such as the magmatic Cu-Ni sulfide deposits. In the study area, two post-

mineralization cooling pulses (late Permian-Early Triassic and Cretaceous, respectively) accelerated the exposure process of the ore body, while the Late Cretaceous-Cenozoic cooling stagnation indicates a period of only limited erosion at most, thus preventing the destruction of the deposit and hence preserving it for the current exploitation. It is suggested that the areas that display a similar thermo-tectonic history in the Chinese Eastern Tianshan are probably also potential targets of ore deposit exploration.

## Declaration of Competing Interest

The authors declare that they have no known competing financial interests or personal relationships that could have appeared to influence the work reported in this paper.

## Data availability

The data that has been used is confidential.

## Acknowledgments

We are grateful to two anonymous reviewers for their insightful suggestions that greatly improved the manuscript, and Associate Editor Jiyuan Yin and Editor-in-Chief Huayong Chen for efficient editorial handling. This study was financially supported by the National Natural Science Foundation of China (Grant No. 92162211) and the National Key R&D Plan of China (Grant No.2018YFC0603703).

## References

- Allen, M.B., Anderson, L., Searle, R.C., Buslov, M., 2006. Oblique rift geometry of the West Siberian Basin: tectonic setting for the Siberian flood basalts. *J. Geol. Soc.* 163 (6), 901–904.
- Ao, S.J., Xiao, W.J., Han, C.M., Mao, Q.G., Zhang, J.E., 2010. Zircon U-Pb age, geochemistry and Hf isotopes of the early Permian mafic-ultramafic complexes in the Beishan area, NW China: implications for the late Paleozoic tectonic evolution of the Altaiids. *Gondw. Res.* 18, 466–478.
- Avouac, J.P., Tapponnier, P., Bai, P., You, H., Wang, G., 1993. Active thrusting and folding along the northern Tien Shan, and Late Cenozoic rotation of the Tarim relative to the Junggar and Kazakhstan. *J. Geophys. Res.* 98, 6755–6804.
- Beucher, R., Brown, R.W., Roper, S., Stuart, F., Persano, C., 2013. Natural age dispersion arising from the analysis of broken crystals: Part II. Practical application to apatite (U-Th)/He thermochronometry. *Geochim. Cosmochim. Acta* 120, 395–416.
- Burchfiel, B.C., Brown, E.T., Deng, Q.D., Feng, X.Y., Li, J., Molnar, P., Shi, J.B., Wu, Z.M., You, H.C., 1999. Crustal shortening on the margins of the Tien Shan, Xinjiang, China. *Int. Geol. Rev.* 41, 665–700.
- Carlson, W.D., Donelick, R.A., Ketcham, R.A., 1999. Variability of apatite fission-track annealing kinetics: I. Experimental results. *Am. Mineral.* 84, 1213–1223.
- Charvet, J., Shu, L.S., Laurent-Charvet, S., 2007. Paleozoic structural and geodynamic evolution of eastern Tianshan (NW China): welding of the Tarim and Junggar plates.  *Episodes* 30, 162–186.
- Chen, Y., Wang, G.C., Kapp, P., Shen, T.Y., Zhang, P., Zhu, C.Y., Cao, K., 2020. Episodic exhumation and related tectonic controlling during Mesozoic in the Eastern Tian Shan, Xinjiang, northwestern China. *Tectonophysics* 796, 228647.
- Chen, H.Y., Yang, J.T., Baker, M., 2012. Mineralization and fluid evolution of the Jiyuan polymetallic Cu-Ag-Pb-Zn-Au deposit, eastern Tianshan, NW China. *Int. Geol. Rev.* 54, 816–832.
- Cunningham, D., Owen, L., Snee, L., Li, J., 2003. Structural framework of a major intracontinental orogenic termination zone: The easternmost Tien Shan, China. *J. Geol. Soc.* 160, 575–590.
- De Grave, J., Glorie, S., Buslov, M.M., Stockli, D.F., McWilliams, M.O., Batalev, Yu, V., Van den haute, P., 2013. Thermo-tectonic history of the Issyk-kul basement (Kyrgyz northern Tien Shan, Central Asia). *Gondwana Res.* 23, 998–1020.
- De Grave, J., Glorie, S., Buslov, M.M., Izmer, A., Fournier-Carrie, A., Batalev, V.Y., Vanhaecke, F., Elburg, M.A., Van den Haute, P., 2011. The thermo-tectonic history of the Song-Kul Plateau, Kyrgyz Tien Shan: constraints by apatite and titanite thermochronometry and zircon U/Pb dating. *Gondw. Res.* 20 (4), 745–763.
- De Pelsmaeker, E., Glorie, S., Buslov, M.M., Zhimulev, F.I., Poujol, M., Korobkin, V.V., Vanhaecke, F., Vetrov, E.V., De Grave, J., 2015. Late-Paleozoic emplacement and Meso-Cenozoic reactivation of the southern Kazakhstan granitoid basement. *Tectonophysics* 662, 416–433.
- Duan, S.G., Jiang, Z.S., Zhang, Z.H., Li, F.M., Ren, Y.Q., 2017. Re-Os isotopic analysis of pyrrhotite from Tianyu Cu-Ni sulfide deposit in Eastern Tianshan Mountains, Xinjiang: Constraints on sources of ore-forming material. *Miner. Depos.* 36, 25–37 in Chinese with English abstract.
- Dumitru, T.A., Zhou, D., Chang, E.Z., Graham, S.A., 2001. Uplift, exhumation, and deformation in the Chinese Tian Shan. *Memoir. Geol. Soc. Am.* 194, 71–99.

- Enkelmann, E., Garver, J.I., 2016. Low-temperature thermochronology applied to ancient settings. *J. Geod.* 93, 17–30.
- Evans, N.J., McInnes, B.I., McDonald, B., Danišík, M., Jourdan, F., Mayers, C., Thern, E., Corbett, D., 2013. Emplacement age and thermal footprint of the diamondiferous Ellendale E9 lamproite pipe, Western Australia. *Miner. Deposita* 48, 413–421.
- Fang, Y., Wu, C.D., Wang, Y.Z., Hou, K.J., Guo, Z.J., 2019a. Topographic evolution of the Tianshan Mountains and their relation to the Junggar and Turpan Basins, Central Asia, from the Permian to the Neogene. *Gondw. Res.* 75, 47–67.
- Fang, L.R., Tang, D.M., Qin, K.Z., Niu, Y.J., Mao, Y.J., Kang, Z., 2019b. The indicative significance of amphibole composition to magmatic process of copper-nickel deposits in eastern Tianshan. *Acta Petrol. Sin.* 35 (7), 2061–2085 in Chinese with English Abstract.
- Farley, K.A., 2000. Helium diffusion from apatite: General behavior as illustrated by Durango fluorapatite. *J. Geophys. Res. Solid Earth* 105, 2903–2914.
- Farley, K.A., Wolf, R.A., Silver, L.T., 1996. The effects of long alpha-stopping distances on (U-Th)/He ages. *Geochim. Cosmochim. Acta* 60, 4223–4229.
- Fitzgerald, P.G., Baldwin, S.L., Webb, L.E., O'Sullivan, P.B., 2006. Interpretation of (U-Th)/He single grain ages from slowly cooled crustal terranes: A case study from the Transantarctic Mountains of southern Victoria Land. *Chem. Geol.* 225, 91–120.
- Flowers, R.M., Kelley, S.A., 2011. Interpreting data dispersion and “inverted” dates in apatite (U-Th)/He and fission-track datasets: An example from the US midcontinent. *Geochim. Cosmochim. Acta* 75, 5169–5186.
- Galbraith, R.F., Green, P.F., 1990. Estimating the component ages in a finite mixture. *International Journal of Radiation Applications and Instrumentation. Part D. Nucl. Tracks. Radiat. Meas.* 17 (3), 197–206.
- Gallagher, K., 2012. Transdimensional inverse thermal history modeling for quantitative thermochronology. *J. Geophys. Res. Solid Earth* 117, 1–16.
- Gallagher, K., Brown, R., Johnson, C., 1998. Fission track analysis and its applications to geological problems. *Annu. Rev. Earth Planet. Sci.* 26, 519–572.
- Gallagher, K., Charvin, K., Nielsen, S., Sambridge, M., Stephenson, J., 2009. Markov chain Monte Carlo (MCMC) sampling methods to determine optimal models, model resolution and model choice for Earth Science problems. *Marine. Petrol. Geol.* 26, 525–535.
- Gao, J., Klemd, R., Zhu, M., Wang, X., Li, J., Wan, B., Xiao, W., Zeng, Q., Shen, P., Sun, J., Qin, K., Campos, E., 2018. Large-scale porphyry-type mineralization in the Central Asian metallogenic domain: A review. *J. Asian Earth Sci.* 165, 7–36.
- Gillespie, J., Glorie, S., Jepson, G., Zhang, Z.Y., Xiao, W.J., Danišík, M., Collins, A.S., 2017a. Differential exhumation and crustal tilting in the easternmost Tianshan (Xinjiang, China), revealed by low-temperature thermochronology. *Tectonics* 36, 2142–2158.
- Gillespie, J., Glorie, S., Xiao, W.J., Zhang, Z.Y., Collins, A.S., Evans, N., McInnes, B., De Grave, J., 2017b. Mesozoic reactivation of the Beishan, southern Central Asian Orogenic Belt: Insights from low-temperature thermochronology. *Gondw. Res.* 43, 107–122.
- Gleadlow, A., Harrison, M., Kohn, B., Lugo-Zazueta, R., Phillips, D., 2015. The Fish Canyon Tuff: A new look at an old low-temperature thermochronology standard. *Earth Planet. Sci. Lett.* 424, 95–108.
- Glorie, S., De Grave, J., 2016. Exhuming the Meso-Cenozoic Kyrgyz Tianshan and Siberian Altai-Sayan: a review based on low-temperature thermochronology. *Geosci. Front.* 7, 155–170.
- Glorie, S., Otasevic, A., Gillespie, J., Jepson, G., Danišík, M., Zhimulev, F.I., et al., 2019. Thermo-tectonic history of the Junggar Alatau within the Central Asian Orogenic belt (SE Kazakhstan, NW China): insights from integrated apatite U/Pb, fission track and (U-Th)/He thermochronology. *Geosci. Front.* 10, 2153–2166.
- Gong, L., Kohn, B., Zhang, Z.Y., Xiao, B., Wu, L., Chen, H.Y., 2021. Preservation of Paleozoic Porphyry Cu Deposits: Insights from the Yandong Deposit, Southern Central Asian Orogenic Belt. *Econ. Geol.* 116 (3), 607–628.
- Guenther, W.R., Reiners, P.W., Ketcham, R.A., Nasdala, L., Giesler, G., 2013. Helium diffusion in natural zircon: Radiation damage, anisotropy, and the interpretation of zircon (U-Th)/He thermochronology. *Am. J. Sci.* 313, 145–198.
- Han, B.F., Guo, Z.J., Zhang, Z.C., Zhang, L., Chen, J.F., Song, B., 2010a. Age, geochemistry, and tectonic implications of a late Paleozoic stitching pluton in the North Tian Shan suture zone, western China. *Geol. Soc. Am. Bull.* 122, 627–640.
- Han, C.M., Xiao, W.J., Zhao, G.C., Ao, S.J., Zhang, J., Qu, W.J., Du, A.D., 2010b. In-situ U-Pb, Hf and Re-Os isotopic analyses of the Xiangshan Ni-Cu-Co deposit in Eastern Tianshan (Xinjiang), Central Asia Orogenic Belt: Constraints on the timing and genesis of the mineralization. *Lithos* 120 (3–4), 547–562.
- Han, Y.G., Zhao, G.C., 2018. Final amalgamation of the Tianshan and Junggar orogenic collage in the southwestern Central Asian Orogenic Belt: constraints on the closure of the Paleo-Asian Ocean. *Earth Sci. Rev.* 186, 129–152.
- Hao, L., Wang, Y.M., Xin, R.C., Wang, Y., 2006. Study on the slope break belts in the Jurassic down-warped lacustrine basin in western-margin area, Junggar Basin, northwestern China. *Mar. Petr. Geol.* 23, 913–930.
- He, Z.Y., 2022. Intra-continental evolution of the Chinese Tianshan and Junggar orogenic collage. Ghent University, pp. 1–314. PhD thesis.
- He, Z.Y., Klemd, R., Zhang, Z.M., Zong, K.Q., Sun, L.X., Tian, Z.L., Huang, B.T., 2015. Mesoproterozoic continental arc magmatism and crustal growth in the eastern Central Tianshan arc terrane of the southern Central Asian Orogenic Belt: geochronological and geochemical evidence. *Lithos* 236, 74–89.
- He, Z.Y., Wang, B., Ni, X.H., De Grave, J., Scaillet, S., Chen, Y., Liu, J.S., Zhu, X., 2021a. Structural and kinematic evolution of strike-slip shear zones around and in the Central Tianshan: insights for eastward tectonic wedging in the southwest Central Asian Orogenic Belt. *J. Struct. Geol.* 144, 104279.
- He, Z.Y., Wang, B., Nachtergaelie, S., Glorie, S., Ni, X.H., Su, W.B., Cai, D.X., Liu, J.S., De Grave, J., 2021b. Long-term topographic evolution of the Central Tianshan (NW China) constrained by low-temperature thermochronology. *Tectonophysics* 817, 229066.
- He, Z.Y., Wang, B., Glorie, S., Su, W.B., Ni, X.H., Jepson, G., Liu, J.S., Zhong, L.L., Gillespie, J., De Grave, J., 2022a. Mesozoic building of the Eastern Tianshan and East Junggar (NW China) revealed by low-temperature thermochronology. *Gondw. Res.* 103, 37–53.
- He, Z.Y., Glorie, S., Wang, F.J., Zhu, W.B., Fonseca, A., Su, W.B., Zhong, L.L., Zhu, X., De Grave, J., 2022b. A re-evaluation of the Meso-Cenozoic thermo-tectonic evolution of Bogda Shan (Tian Shan, NW China) based on new basement and detrital apatite fission track thermochronology. *Int. Geol. Rev.* <https://doi.org/10.1080/00206814.2022.2121946>.
- He, Z.Y., Wang, B., Su, W.B., Glorie, S., Ni, X.H., Liu, J.S., Cai, D.X., Zhong, L.L., De Grave, J., 2022c. Meso-Cenozoic thermo-tectonic evolution of the Yili block within the Central Asian Orogenic Belt (NW China): Insights from apatite fission track thermochronology. *Tectonophysics* 823, 229194.
- Heinhorst, J., Lehmann, B., Ermolov, P., Serykh, V., Zhurutin, S., 2000. Paleozoic crustal growth and metallogeny of Central Asia: evidence from magmatic-hydrothermal ore systems of Central Kazakhstan. *Tectonophysics* 328, 69–87.
- House, M.A., Farley, K.A., Stockli, D., 2000. Helium chronometry of apatite and titanite using Nd-YAG laser heating. *Earth Planet. Sci. Lett.* 83, 365–368.
- Hu, A.Q., Wei, G.J., Jahn, B.M., Zhang, J.B., Deng, W.F., Chen, L.L., 2010. Formation of the 0.9 Ga Neoproterozoic granitoids in the Tianshan Orogen, NW China: constraints from the SHRIMP zircon age determination and its tectonic significance. *Geochimica* 39, 197–212 in Chinese with English abstract.
- Huang, Z.Y., Long, X.P., Kröner, A., Yuan, C., Wang, Y.J., Chen, B., Zhang, Y.Y., 2015. Neoproterozoic granitic gneisses in the Chinese Central Tianshan Block: implications for tectonic affinity and Precambrian crustal evolution. *Precambr. Res.* 269, 73–89.
- Jahn, B.M., Windley, B., Natal' in, B., Dobretsov, N., 2004. Phanerozoic continental growth in Central Asia. *J. Asian Earth Sci.* 23, 599–603.
- Jolivet, M., Dominguez, S., Charreau, J., Chen, Y., Li, Y., Wang, Q., 2010. Mesozoic and Cenozoic tectonic history of the central Chinese Tian Shan: reactivated tectonic structures and active deformation. *Tectonics* 29, TC6019.
- Jolivet, M., Heilbron, G., Robin, C., Barrier, L., Bourquin, S., Guo, Z., Jia, Y., Guerit, L., Yang, W., Fu, B., 2013. Reconstructing the Late Palaeozoic-Mesozoic topographic evolution of the Chinese Tian Shan: available data and remaining uncertainties. *Adv. Geosci.* 37, 7–18.
- Jolivet, M., Barrier, L., Dauteuil, O., Laborde, A., Li, Q., Reichenbacher, B., Guo, Z., et al., 2018. Late Cretaceous-Palaeogene topography of the Chinese Tian Shan: New insights from geomorphology and sedimentology. *Earth Planet. Sci. Lett.* 499, 95–106.
- Kapp, P., DeCelles, P., 2019. Mesozoic-Cenozoic geological evolution of the Himalayan Tibetan orogen and working tectonic hypothesis. *Am. J. Sci.* 319 (3), 159–254.
- Kesler, S.E., Wilkinson, B.H., 2006. The role of exhumation in the term portal distribution of ore deposits. *Econ. Geol.* 101 (5), 919–922.
- Ketcham, R.A., Donelick, R.A., Carlson, W.D., 1999. Variability of apatite fission-track annealing kinetics: III. Extrapolation to geological time scales. *Am. Mineral.* 84 (9), 1235–1255.
- Lei, R.X., Wu, C.Z., Chi, G.X., Gu, L.X., Dong, L.H., Qu, X., Jiang, Y.H., Jiang, S.Y., 2013. The Neoproterozoic Honglujing A-type granite in Central Tianshan (NW China): LA-ICP-MS zircon U-Pb geochronology, geochemistry, Nd-Hf isotope and tectonic significance. *J. Asian Earth Sci.* 74, 142–154.
- Li, Z.Y., Ding, L., Lippert, P.C., Song, P.P., Yue, Y.H., van Hinsbergen, D.J.J., 2016. Paleomagnetic constraints on the Mesozoic drift of the Lhasa terrane (Tibet) from Gondwana to Eurasia. *Geology* 44, 727–730.
- Li, G.W., Sandiford, M., Fang, A.M., Kohn, B., Sandiford, D., Fu, B.H., Zhang, T.L., Cao, Y., Chen, F., 2019. Multi-stage exhumation history of the West Kunlun orogen and the amalgamation of the Tibetan Plateau. *Earth Planet. Sci. Lett.* 528, 115833.
- Mao, J.W., Konopelko, D., Seltmann, R., Lehmann, B., Chen, W., Wang, Y.T., Eklund, O., Usubaliev, T., 2004. Postcollisional age of the Kumtor gold deposit and timing of Hercynian events in the Tien Shan. *Kyrgyzstan. Econ. Geol.* 99, 1771–1780.
- Mao, J.W., Pirajno, F., Zhang, Z.H., Chai, F.M., Wu, H., Chen, S.P., Cheng, L.S., Yang, J.M., Zhang, C.Q., 2008. A review of the Cu-Ni sulphide deposits in the Chinese Tianshan and Altay orogens (Xinjiang Autonomous Region, NW China): principal characteristics and ore-forming processes. *J. Asian Earth Sci.* 32 (2–4), 184–203.
- Mao, Y.J., Qin, K.Z., Li, C., Tang, D.M., 2015. A modified genetic model for the Huangshandong magmatic sulfide deposit in the Central Asian Orogenic Belt, Xinjiang, western China. *Miner. Deposita* 50, 65–82.
- Márton, I., Moritz, R., Spikings, R., 2010. Application of low-temperature thermochronology to hydrothermal ore deposits: formation, preservation and exhumation gold system from the Eastern Rhodopes, Bulgaria. *Tectonophysics* 483, 240–254.
- McInnes, B.I.A., Evans, N.J., Fu, F.Q., Garwin, S., 2005. Application of thermochronology to hydrothermal ore deposits. *Rev. Miner. Geochem.* 58, 467–498.
- Morin, J., Jolivet, M., Barrier, L., Laborde, A., Li, H.B., Dauteuil, O., 2019. Planation surfaces of the Tian Shan Range (Central Asia): Insight on several 100 million years of topographic evolution. *J. Asian Earth Sci.* 177, 52–65.
- Muhtar, M.N., Wu, C.Z., Brzozowski, M.J., Yuan, X.C., Li, P., Wang, S.M., Zhi, J., Jiang, Y.H., 2020. Geochronology, geochemistry, and Sr-Nd-Pb-Hf-S isotopes of wall rocks from the Kangjur gold polymetallic deposit, Chinese North Tianshan: Implications for petrogenesis and sources of ore-forming materials. *Ore Geol. Rev.* 125, 103688.
- Nachtergaelie, S., De Pelsmaeker, E., Glorie, S., Zhimulev, F., Jolivet, M., Danišík, M., Buslov, M.M., De Grave, J., 2018. Meso-Cenozoic tectonic evolution of the Tala-Fergana region of the Kyrgyz Tien Shan revealed by low-temperature basement and detrital thermochronology. *Geosci. Front.* 9, 1495–1514.

- Pirajno, F., 2010. Intracontinental strike-slip faults, associated magmatism, mineral systems and mantle dynamics: examples from NW China and Altay-Sayan (Siberia). *J. Geod.* 50, 325–346.
- Qin, K.Z., Su, B.X., Sakyi, P.A., Tang, D.M., Li, X.H., Sun, H., Xiao, Q.H., Liu, P.P., 2011. SIMS zircon U-Pb geochronology and Sr-Nd isotopes of Ni-Cu-Bearing MaficUltramafic Intrusions in Eastern Tianshan and Beishan in correlation with flood basalts in Tarim Basin (NW China): Constraints on a ca. 280 Ma mantle plume. *Am. J. Sci.* 311 (3), 237–260.
- Reiners, P.W., Brandon, M.T., 2006. Using thermochronology to understand orogenic erosion. *Annu. Rev. Earth Planet Sci.* 34, 419–466.
- Reiners, P.W., Farley, K.A., 2001. Influence of crystal size on apatite (U-Th)/He thermochronometry: An example from the Bighorn Mountains, Wyoming. *Earth Planet. Sci. Lett.* 188, 413–420.
- Reiners, P.W., Spell, T.L., Nicolescu, S., Zanetti, K.A., 2004. Zircon (U-Th)/He thermochronometry: He diffusion and comparisons with  $^{40}\text{Ar}/^{39}\text{Ar}$  dating. *Geochim. Cosmochim. Acta* 68 (8), 1857–1887.
- Selmann, R., Porter, T.M., Pirajno, F., 2014. Geodynamics and metallogeny of the central Eurasian porphyry and related epithermal mineral systems: A review. *J. Asian Earth Sci.* 79, 810–841.
- Shen, P., Pan, H.D., Seitmuratova, E., Jakupova, S., 2016. U-Pb zircon, geochemical and Sr-Nd-Hf-O isotopic constraints on age and origin of the ore-bearing intrusions from the Nurkazgan porphyry Cu-Au deposit in Kazakhstan. *J. Asian Earth Sci.* 116, 232–248.
- Shu, L.S., Charvet, J., Guo, L.Z., Lu, H.F., Laurent-Charvet, S., 1999. A large-scale Palaeozoic dextral ductile strike-slip zone: the Aqqikhudug-Weiye zone along the northern margin of the Central Tianshan belt, Xinjiang, NW China. *Acta Geol. Sin.* 73, 148–162.
- Shu, L.S., Charvet, J., Lu, H.F., Laurent, S.C., 2002. Paleozoic accretion-collision events and kinematics of ductile deformation in the eastern part of the southern-central Tianshan belt, China. *Acta Geol. Sin.* 76, 308–323.
- Shu, L.S., Lu, H.F., Yin, D.H., Wang, B., 2003. Paleozoic accretion-collision events and kinematics of ductile deformation in the Central-Southern Tianshan belt. *J. Nanjing Univ. (Natural Sciences)* 39, 17–30 in Chinese with English abstract.
- Shu, L.S., Yu, J.H., Charvet, J., Laurent-Charvet, S., Zhang, R.G., Sang, H.Q., 2004. Isotopic dating and geochemical constraint: granulite features in the eastern part of the Tianshan Belt, NW China. *J. Asian Earth Sci.* 24 (1), 25–41.
- Sun, J.B., Chen, W., Qin, K.Z., Danisik, M., Evans, N., McInnes, B., Shen, Z., Zhao, Sh.f., Zhang, B., Yin, J.Y., Tao, N., 2021. Mesozoic exhumation of the Jueltuotage area, Eastern Tianshan, NW China: constraints from (U-Th)/He and fission-track thermochronology. *Geol. Mag.* 1–17.
- Suzuki, K., Shimizu, H., Masuda, A., 1996. Re-Os dating of molybdenites from ore deposits in Japan: implication for the closure temperature of the Re-Os system for molybdenite and the cooling history of molybdenum ore deposits. *Geochim. Cosmochim. Acta* 60, 3151–3315.
- Tang, D.M., Qin, K.Z., Sun, H., Qi, L., Xiao, Q.H., Su, B.X., 2009. PGE Geochemical Characteristics of Tianyu Magmatic Cu-Ni Deposit: Implications for Magma Evolution and Sulfide Segregation. *Acta Geol. Sin.* 83, 681–697 in Chinese with English abstract.
- Tang, D.M., Qin, K.Z., Li, C.S., Qi, L., Su, B.X., Qu, W.J., 2011. Zircon dating, Hf-Sr-Nd-Os isotopes and PGE geochemistry of the Tianyu sulfide-bearing mafic-ultramafic intrusion in the Central Asian Orogenic Belt, NW China. *Lithos* 126, 84–98.
- Tang, D.M., Qin, K.Z., Sun, H., Su, B.X., Xiao, Q.H., 2012. The role of crustal contamination in the formation of Ni-Cu sulfide deposits in Eastern Tianshan, Xinjiang, Northwest China: Evidence from trace element geochemistry, Re-Os, Sr-Nd, zircon Hf-O, and sulfur isotopes. *J. Asian Earth Sci.* 49, 145–160.
- Vassallo, R., Jolivet, M., Ritz, J.-F., Braucher, R., Larroque, C., Sue, C., Toddbieg, M., Javkhlanbold, D., 2007. Uplift age and rates of the Gurvan Bogd system (Gobi-Altay) by apatite fission track analysis. *Earth Planet. Sci. Lett.* 259 (3), 333–346.
- Wan, B., Xiao, W.J., Windley, B.F., Gao, J., Zhang, L.C., Cai, K.D., 2017. Contrasting ore styles and their role in understanding the evolution of the Altaiids. *Ore Geol. Rev.* 8, 910–922.
- Wang, Y.N., Cai, K.D., Sun, M., Xiao, W.J., De Grave, J., Wan, B., Bao, Z.H., 2018. Tracking the multi-stage exhumation history of the western Chinese Tianshan by Apatite Fission Track (AFT) dating: Implications for the preservation of epithermal deposits in the ancient orogenic belt. *Ore Geol. Rev.* 100, 111–132.
- Wang, Y.N., Cai, K.D., Sun, M., Bao, Z.H., 2021. Burial and exhumation of late paleozoic arc-related rocks in the Tulasu basin, Western Chinese Tianshan: Implication for the preservation of epithermal deposits in old orogenic belts. *Gondw. Res.* 97, 51–67.
- Wang, B., Faure, M., Cluzel, D., Shu, L.S., Charvet, J., Meffre, S., Ma, Q., 2006. Late Palaeozoic tectonic evolution of the northern West Chinese Tianshan Belt. *Geod. Acta* 19, 237–247.
- Wang, B., Shu, L., Faure, M., Jahn, B.M., Cluzel, D., Charvet, J., Chung, S.L., Meffre, S., 2011. Paleozoic tectonics of the southern Chinese Tianshan: Insights from structural, chronological and geochemical studies of the Heiyingshan ophiolitic mélange (NW China). *Tectonophysics* 497, 85–104.
- Wang, B., Cluzel, D., Jahn, B.-M., Shu, L., Chen, Y., Zhai, Y., Branquet, Y., Barbanson, L., Sizaret, S., 2014. Late Paleozoic pre- and syn-kinematic plutons of the Kangguer-Huangshan Shear zone: inference on the tectonic evolution of the eastern Chinese north Tianshan. *Am. J. Sci.* 314, 43–79.
- Wang, X.S., Klemd, R., Gao, J., Jiang, T., Li, J.L., Xue, S.C., 2018. Final assembly of the Southwestern Central Asian Orogenic Belt as constrained by the evolution of the South Tianshan Orogen: Links with Gondwana and Pangea. *J. Geophys. Res. Solid Earth* 123, 7361–7388.
- Wang, Y., Li, J.Y., Sun, G.H., 2008b. Postcollisional eastward extrusion and tectonic exhumation along the eastern Tianshan Orogen, Central Asia: constraints from dextral strike-slip motion and  $^{40}\text{Ar}/^{39}\text{Ar}$  geochronological evidence. *J. Geol.* 116, 599–618.
- Wang, H., Qu, W.J., Li, H.Q., Chen, S.P., 2007. Dating and discussion on the rock-forming and ore-forming age of newly-discovered Cu-Ni-sulfide deposits in Hami, Xinjiang. *Acta Geol. Sinica* 81 (4), 526–530 in Chinese with English abstract.
- Wang, Y., Sun, G.H., Li, J.Y., 2009. U-Pb (SHRIMP) and  $^{40}\text{Ar}/^{39}\text{Ar}$  geochronological constraints on the evolution of the Xingxingxia shear zone, NW China: a Triassic segment of the Altyn Tagh fault system. *Geol. Soc. Am. Bull.* 122, 487–505.
- Wang, J., Zhai, Y., Liu, J., Liu, Z., Liu, J., 2008a. A new approach to post-ore change and preservation of ore deposits: Fission track analysis. *Adv. Earth Science* 23, 421–427 in Chinese with English abstract.
- Wang, Y.Q., Zhu, W.B., Luo, M., 2022. Tectono-thermal Chronology of the Xingxingxia Complex in Eastern Tianshan. *Geol. J. China Univ.* 28, 582–591 in Chinese with English abstract.
- Wen, D.J., He, Z.Y., Zhang, M.Z., 2019. Geochemistry and tectonic implications of Early Permian granitic rocks in the Xingxingxia area of Chinese Central Tianshan Arc Terrane. *Geol. J.* 54, 1578–1590.
- Wilhem, C., Windley, B.F., Stampfli, G.M., 2012. The Altaiids of Central Asia: a tectonic and evolutionary innovative review. *Earth Sci. Rev.* 113, 303–341.
- Windley, B.F., Alexeev, D., Xiao, W.J., Kröner, A., Badarch, G., 2007. Tectonic models for accretion of the Central Asian Orogenic Belt. *J. Geol. Soc. London* 164, 31–47.
- Wu, C.Z., Xie, S.W., Gu, L.X., Samson, I.M., Yang, T., Lei, R.X., Zhu, Z.Y., Dang, B., 2018. Shear zone-controlled post-magmatic ore formation in the Huangshandong Ni-Cu sulfide deposit, NW China. *Ore Geol. Rev.* 100, 545–560.
- Xbgmr, 1993. Regional Geology of Xinjiang Uygur Autonomy Region. Geological Publishing House, Beijing.
- Xiao, B., Chen, H., Hollings, P., Han, J., Wang, Y., Yang, J., Cai, K., 2017. Magmatic evolution of the Tuwu-Yandong porphyry Cu belt, NW China: Constraints from geochronology, geochemistry and Sr-Nd-Hf isotopes. *Gondw. Res.* 43, 74–91.
- Xiao, W.J., Windley, B.F., Hao, J., Zhai, M.G., 2003. Accretion leading to collision and the Permian Solonker suture, Inner Mongolia, China: termination of the Central Asian orogenic belt. *Tectonics* 22, 1069.
- Xiao, W.J., Zhang, L.C., Qin, K.Z., Sun, S., Li, J.L., 2004. Paleozoic accretionary and collisional tectonics of the Eastern Tianshan (China): implications for the continental growth of central Asia. *Am. J. Sci.* 304, 370–395.
- Xiao, W.J., Windley, B.F., Yuan, C., Sun, M., Han, C.M., Lin, S.F., Chen, H.L., Yan, Q.R., Liu, D.Y., Qin, K.Z., Li, J.L., Sun, S., 2009. Paleozoic multiple subduction-accretion processes of the southern Altaiids. *Am. J. Sci.* 309, 221–270.
- Xiao, W.J., Mao, Q.G., Windley, B.F., Qu, J.F., Zhang, J.E., Ao, S.J., Guo, Q.Q., Cleven, N. R., Lin, S.F., Shan, Y.H., Li, J.L., 2010. Paleozoic multiple accretionary and collisional processes of the Beishan orogenic collage. *Am. J. Sci.* 310, 1553–1594.
- Xiao, W.J., Song, D.F., Windley, B.F., Li, J.L., Han, C.M., Wan, B., Zhang, J.E., Ao, S.J., Zhang, Z.Y., 2020. Accretionary processes and metallogenesis of the Central Asian Orogenic Belt: Advances and perspectives. *Sci. China Earth Sci.* 63, 329–361.
- Yakubchuk, A., 2004. Architecture and mineral deposit settings of the Altaiid orogenic collage: a revised model. *J. Asian Earth Sci.* 23, 761–779.
- Yin, J.Y., Chen, W., Hodges, K.V., Xiao, W.J., Cai, K.D., Yuan, C., Sun, M., Liu, L.P., van Soest, M., 2018. The thermal evolution of Chinese central Tianshan and its implications: insights from multi-method chronometry. *Tectonophysics* 722, 536–548.
- Yin, J.Y., Chen, W., Thomson, S.N., Sun, M., Wang, Y.N., Xiao, W.J., Yuan, C., Sun, J.B., Long, X.P., 2019. Fission track thermochronology of the Tuwu-Yandong porphyry Cu deposits, NW China: Constraints on preservation and exhumation. *Ore Geol. Rev.* 113, 103104.
- Yin, A., Harrison, T.M., 2000. Geologic evolution of the Himalayan-Tibetan orogen. *Annu. Rev. Earth Planet. Sci.* 28, 211–280.
- Yin, A., Nie, S., Craig, P., Harrison, T.M., Ryerson, F.J., Xianglin, Q., Geng, Y., 1998. Late Cenozoic tectonic evolution of the southern Chinese Tian Shan. *Tectonics* 17, 1–27.
- Zeng, Q.D., Sun, Y., Chu, S.X., Duan, X.X., Liu, J.M., 2015. Geochemistry and geochronology of the Dongshanwan porphyry Mo-W deposit, Northeast China: implications for the Late Jurassic tectonic setting. *J. Asian Earth Sci.* 97, 472–485.
- Zhai, Y.S., Deng, J., Peng, R.M., 2000. Research contents and methods for post-ore changes, modifications and preservation. *Earth Sci.: J. China Univ. Geosci.* 25 (4), 340–345 in Chinese with English abstract.
- Zhang, L., Yang, L.Q., Wang, Y., Weinberg, R.F., An, P., Chen, B.Y., 2017. Thermochronologic constrains on the processes of formation and exhumation of the Xinli orogenic gold deposit, Jiaodong Peninsula, eastern China. *Ore Geol. Rev.* 81, 140–153.
- Zhang, X., Zhao, G., Sun, M., Eizenhöfer, P.R., Han, Y., Hou, W., Liu, D., Wang, B., Liu, Q., Xu, B., 2016. Tectonic evolution from subduction to arc-continent collision of the Junggar ocean: constraints from U-Pb dating and Hf isotopes of detrital zircons from the North Tianshan belt, NW China. *Geol. Soc. Am. Bull.* 128, 644–660.
- Zhong, L.L., Wang, B., de Jong, K., Zhai, Y.Z., Liu, H.S., 2019. Deformed continental arc sequences in the south Tianshan: new constraints on the early Paleozoic accretionary tectonics of the Central Asian Orogenic Belt. *Tectonophysics* 768, 228169.
- Zhou, M.F., Leshner, C.M., Yang, Z., Li, J., Sun, M., 2004. Geochemistry and petrogenesis of 270 Ma Ni-Cu-(PGE) sulfide-bearing mafic intrusions in the Huangshan district, Eastern Xinjiang, Northwest China: implications for the tectonic evolution of the Central Asian orogenic belt. *Chem. Geol.* 209 (3–4), 233–257.